1

=======

Machine Learning Methods for Cross Section Measurements

by

Krish Desai

A dissertation submitted in partial satisfaction of the

requirements for the degree of

Doctor of Philosophy

in

Physics

in the

Graduate Division

of the

University of California, Berkeley

Committee in charge:

Professor Benjamin Nachman, Co-chair
Professor Uros Seljak, Co-chair
Professor Joshua Bloom
Professor Saul Perlmutter

Summer 2025

Machine Learning Methods for Cross Section Measurements

To Ben Nachman,

my advisor, mentor, and friend.

Contents

Contents ii

List of Figures xxx

List of Tables xli

I Introduction and physics background. 1

I.A Units and conventions. 2

I.A.1 Coordinate systems and relativistic geometry. 3

I.A.2 Statistical frameworks and uncertainty quantification. 7

I.A.3 Machine learning architectures and notation. 8

I.A.4 Information theory and optimal observables. 9

I.A.5 A note on conventions and clarity. 10

I.B The Standard Model: Theoretical framework. 11

I.B.1 Fundamental particles and forces. 13

I.B.1.i Fermions: The building blocks of matter. 13

I.B.1.i.a Quarks. 13

I.B.1.i.b Leptons. 14

I.B.1.ii Bosons: Force carriers. 15

I.B.2 Theoretical framework and symmetries. 16

I.B.3 The Higgs mechanism and mass generation. 17

I.B.4 Limitations and beyond the Standard Model (BSM) physics. 18

I.C Fundamental role of cross section measurements in particle physics. 20

I.D Cross section measurements: From theory to experiment. . 23

I.D.1 Theory. 23

I.D.2 Experimental Measurement 26

I.D.3 Applications in particle physics. 28

I.D.3.i Theory validation. 28

I.D.3.ii Monte Carlo tuning. 29

I.D.3.iii Consistency checks. 31

I.D.3.iv Luminosity determination. 32

I.D.3.v Background estimation. 33

I.D.3.vi Parton luminosity. 33

I.D.3.vii Detector performance validation. 34

I.D.3.viii Systematic uncertainty evaluation. 35

I.D.3.ix Future planning. 35

I.E Detector response in precision measurements. 37

I.F Challenges at modern experiments. 43

I.G Thesis Scope and Physics Impact 46

II Theoretical foundations. 49

II.A Statistical formulation of the unfolding problem. 50
II.A.1 The detector response and forward problem. 50
II.A.2 The inverse problem: Unfolding. 51
II.A.3 Likelihood based formulation. 51
II.A.4 Regularisation techniques. 52
II.A.5 Challenges in high dimensional phase spaces. 53
II.A.5.i Binned methods. 53
II.A.5.ii Unbinned methods. 59
II.B Forward and Inverse Problems in HEP 61
II.B.1 Mathematical Formulation 61
II.B.2 Challenges in Inverse Problems 62
II.B.3 HEP Specific Considerations 63
II.C Historical development: From matrix inversion to modern approaches 66
II.D Traditional unfolding methods in experimental analyses. . . 69
II.D.1 Bin by bin correction. 69

II.D.2 Matrix Inversion 70

II.D.3 Iterative Bayesian unfolding 72

II.D.4 Tikhonov Regularization 73

II.D.5 Template Fitting 75

II.D.6 Regularized Poisson Likelihood 76

II.D.7 Summary 76

II.D.8 Regularization: Need, Approaches, and Limitations 77

II.D.8.i The Necessity of Regularization 78

II.D.8.ii Limitations and practical challenges . . . 78

II.D.8.ii.a Subjectivity-objectivity trade-off 78

II.D.8.ii.b High dimensional regimes 79

II.D.8.ii.c Spectrum dependent biases 80

II.E Unbinned Methods: Statistical Considerations 82

II.E.1 Principles and Implementations 82

II.E.1.i Reweighting Methods 83

II.E.1.ii Generative Modeling 85

II.E.2 Statistical Considerations in Unbinned Regimes . . 87

II.E.3 Limitations in Complex Phase Spaces 88

II.E.3.i Model Misspecification 88

II.F Evaluation metrics for unfolding. 91

II.F.1 Statistical metrics for evaluating point estimates. . 92

II.F.1.i Residual based metrics. 92

II.F.1.ii Distributional distance metrics. 95

II.F.2 Uncertainty quantification metrics 97

II.F.2.i Pull distributions 97

II.F.2.ii Coverage properties 99

II.F.2.iii Variance and bias decomposition 100

II.F.3 Evaluation of correlation structure 102

II.F.3.i Covariance Matrix Assessment 102

II.F.3.ii Event–to–event correlation metrics 103

II.F.4 Method specific evaluation metrics 106

II.F.4.i Iterative methods 106

II.F.4.ii Bayesian Methods 106

II.F.5 Practical considerations. 107

III Machine Learning for Unfolding **101**

III.A The Emergence of Machine Learning in Particle Physics . . 102

III.A.1 A Paradigm Shift in Data Analysis 102

III.A.2 Evolution of ML Applications in HEP 104

III.A.2.i Classification Tasks 104

III.A.2.ii Regression and Anomaly Detection 106

III.A.2.iii Generative Models 107

III.A.3 Machine Learning Approaches to Unfolding 108

III.A.4 Early successes and current challenges 110

III.B Introduction to Neural Networks 113

III.B.1 Essential Concepts 113

III.B.1.i Neural Network Fundamentals 113

III.B.1.ii Forward propagation 118

III.B.1.iii Training objectives and loss functions . . 119

III.B.1.iv Backpropagation and parameter learning . 121
III.B.1.v Batching and Training Dynamics 122
III.B.2 Neural Networks as Universal Approximators . . . 122
III.B.2.i Relevance to physics applications 124
III.B.3 Activation Functions, Optimization, and Regularization 126
III.B.3.i Activation Functions 126
III.B.3.ii Optimization Techniques 130
III.B.3.ii.a Gradient Descent 130
III.B.3.ii.b Stochastic Gradient Descent (SGD) 130
III.B.3.ii.c Momentum based methods 131
III.B.3.ii.d Adaptive Methods 131
III.B.3.ii.d.1 AdaGrad 132
III.B.3.ii.d.2 RMSProp 132
III.B.3.ii.e Adam 132
III.B.3.ii.f Learning Rate Scheduling 133
III.B.3.iii Regularisation techniques. 134

III.B.3.iii.a L^p Regularisation 134

III.B.3.iii.b Dropout 134

III.B.3.iii.c Batch Normalization 135

III.C Supervised Learning Approaches for Unfolding 136

III.C.1 Mathematical Framework 136

III.C.2 Statistical Interpretation 138

III.C.3 Types of Supervised Learning 139

III.C.4 Learning and Generalization 140

III.C.5 Evaluation 140

III.C.6 Unfolding as a Supervised Learning Problem 141

III.C.6.i Classification–Based Approaches 142

III.C.6.ii Regression based calibration 143

III.C.6.ii.a Deterministic regression 144

III.C.6.ii.b Probabilistic regression. 144

III.C.7 Regularisation strategies. 145

III.C.8 Advantages and challenges 146

III.D Deep Learning Architectures 148
III.D.1 Convolutional Neural Networks 148
III.D.2 Recurrent Neural Networks 150
III.D.3 Graph neural networks 151
III.D.4 Transformer based architectures 152
III.D.5 Physics informed neural networks 154
III.D.5.i Energy Flow Networks and Particle Flow Networks 155
III.D.5.i.a Relationship to other architectures 158
III.D.5.i.a.1 Deep sets 158
III.D.5.i.a.2 GNNs and transformers 158
III.E Modern Machine Learning Frameworks 161
III.E.1 Generative Models 161
III.E.1.i Variational Autoencoders (VAEs) 163
III.E.1.ii Normalising flows 167
III.E.1.ii.a Mathematical formulation. 168

III.E.1.ii.b Variations. 169
III.E.1.ii.b.1 Conditional normalising flows 169
III.E.1.ii.b.2 Other innovations. 170
III.E.1.ii.c Applications. 171
III.E.1.ii.c.1 Normalising flows for unfolding. 172
III.E.1.ii.d Limitations. 173
III.E.2 Discriminative Models 175
III.E.2.i Training dynamics and optimization . . . 177
III.E.2.ii Applications 178
III.E.2.iii Traditional discriminative architectures . 180
III.E.2.iii.a Support vector machines 181
III.E.2.iii.b Boosted decision trees. 183
III.E.2.iv Discriminative models and deep learning. 186
III.E.2.v Graph Neural Networks 186
III.E.2.v.a Transformer Models 189
III.E.3 Adversarial models. 191

III.E.3.i Generative Adversarial Networks (GANs) 193
III.E.3.i.a Applications 196
III.E.3.i.a.1 GANs for unfolding. 197
III.E.3.i.b Limitations 199
III.E.3.ii Wasserstein GANs. 200
III.E.3.iii Conditional Adversarial Networks 202
III.E.3.iv Other GAN based methods 204
III.E.3.v Adversarial Autoencoders 205
III.E.3.vi Cycle–Consistent Adversarial Networks . 206
III.F Comparative analysis of ML-based unfolding methods. . . 208
III.F.1 Method selection framework. 208
III.F.2 Performance trade offs. 210
III.F.2.i Synthesis of experimental experience. . . . 212
III.F.3 Open challenges and research frontiers. 214
III.G Case studies: ML based unfolding in HEP analyses. 218
III.G.1 OmniFold 218

III.G.2 Neural Posterior Unfolding 220

III.G.3 Invertible neural networks for unfolding 224

III.G.4 Moment Unfolding 225

III.G.5 Reweighting Adversarial Networks (RAN) 227

III.G.6 Schrödinger Bridge Unfolding 228

III.G.7 Unified Neural Folding GAN 230

III.H ML upstream and downstream of unfolding. 233

III.H.1 Uncertainty quantification in ML based unfolding. . 233

III.H.2 Hybrid approaches and integration with simulation. 235

III.H.3 Equivariant networks for physics-informed unfolding. 236

III.H.4 Comparison with traditional methods. 238

III.H.5 Implementation Considerations from Real Experiments 240

IV Neural Posterior Unfolding 241

IV.A Motivation for improved binned unfolding 242

IV.A.1 Degeneracy and Null Spaces in Unfolding 242

IV.A.2 Regularization Limitations 243

IV.B Normalising flows for inverse problems. 246

IV.B.1 A Bayesian perspective on inverse problems. 246

IV.B.2 Conditional normalising flows for inverse problems. 248

IV.C The Neural Posterior Unfolding Algorithm 251

IV.C.1 Statistical foundation 251

IV.C.2 Machine Learning Architecture 253

IV.C.3 Addressing degeneracy with NPU. 255

IV.C.4 Implicit regularisation in NPU. 257

IV.D Numerical results. 260

IV.D.1 2 bin degenerate response example. 260

IV.D.2 Gaussian example. 262

IV.D.2.i Experimental setup 264

IV.D.2.ii Results and comparison 266

IV.D.3 Particle physics example. 270

IV.D.3.i Dataset and Observables 272

IV.D.3.ii Results 273

IV.D.4 Summary of Numerical Results 275
IV.E Beyond binning: the path forward 279

V Moment Unfolding: direct deconvolution of distribution moments 282

V.A Why moments: physics context and QCD calculations . . . 283
V.A.1 The Theoretical Significance of Moments in Physics 283
V.A.2 Moments in QCD Calculations 285
V.A.2.i DGLAP Evolution Equations 285
V.A.2.ii Operator Product Expansion 286
V.A.2.iii Event Shape Moments 287
V.A.3 Experimental Significance of Moments in QCD . . . 288
V.A.4 Applications in Jet Physics 291
V.A.4.i Moments in physics beyond the Standard Model 293
V.A.5 The case for direct Moment Unfolding 294
V.B A GAN like method to unfold moments 296

V.B.1 Boltzmann inspired reweighting 297
V.B.2 Adversarial training framework 298
V.B.3 Mathematical formalism. 301
V.B.4 Theoretical properties. 303
V.B.4.i Connection to the maximum entropy principle 304
V.B.5 Comparison with traditional GAN architectures. . . 304
V.B.6 Practical considerations. 306
V.B.7 Extension to differential measurements. 307
V.B.8 Theoretical foundations in statistical mechanics. . . 308
V.C Machine learning implementation 310
V.C.1 Training Procedure 313
V.C.2 Gradient Updates 314
V.C.3 Implementation details. 315
V.C.4 Extensions to multiple observables. 316
V.C.5 Uncertainty estimation. 318
V.C.6 Validation procedures. 319

V.C.7 Code availability and reproducibility 320
V.D Case studies 322
V.D.1 Gaussian experiments 322
V.D.1.i Experimental Setup 322
V.D.1.ii Results 323
V.D.2 Jet substructure in collider physics 327
V.D.2.i Datasets 327
V.D.2.ii Observables 328
V.D.2.iii Results 330
V.D.3 Momentum dependent unfolding 335
V.D.3.i Inclusive distributions. 337
V.D.3.ii Differential analysis. 338
V.E Comparison with alternative methods. 343
V.F Conclusion. 348
V.F.1 Towards unfolding distributions. 350

VI RAN: Reweighting Adversarial Networks 353

VI.A The need for full spectral measurements. 354
VI.A.1 Motivation: beyond moments and binned spectra. . 354
VI.A.2 Use cases. 361
VI.A.3 Challenges in unfolding full distributions. 367
VI.A.4 Unbinned unfolding approaches. 373
VI.A.5 Addressing challenges. 379
VI.B From moments to complete differential cross section spectra. 388
VI.B.1 Moments and the full probability distribution. . . . 389
VI.B.1.i The maximum entropy principle and exponential families. 391
VI.B.2 Unfolding with moment constraints: classical and modern approaches. 393
VI.B.2.i Linear regularised unfolding (Tikhonov and SVD). 393
VI.B.2.ii Iterative Bayesian unfolding. 395
VI.B.2.iii Entropy-based methods. 396

VI.B.2.iv Unbinned methods through the lens of moments. 398

VI.B.3 Benefits and challenges of Moment Unfolding. . 400

VI.B.4 Extending Moment Unfolding. 404

VI.C Methodology and regularisation. 414

VI.C.1 Historical Approaches to Regularisation 414

VI.C.2 Regularisation in RAN 418

VI.C.2.i Wasserstein GAN 419

VI.C.2.ii Regularising the critic: Lipschitz constraints 424

VI.C.2.iii Regularising the generator: initialisation and activation constraints. 426

VI.C.3 Regularising with MC Prior 434

VI.D Machine learning implementation. 438

VI.D.1 Neural Network Architecture 438

VI.D.2 Adversarial training procedure. 441

VI.D.3 Datasets and preprocessing. 448

VI.D.3.i Gaussian example. 449

VI.D.3.ii Jet substructure dataset 451

VI.D.4 Training, monitoring and validation. 455

VI.E Results 461

VI.E.1 Gaussian model with smearing. 461

VI.E.2 Jet substructure unfolding results. 465

VI.E.2.i Overall performance. 467

VI.E.2.ii Generality of results 477

VII Unbinned Inference on Correlated Data 480

VII.A Introduction. 481

VII.B Statistical independence in HEP. 483

VII.B.1 Poisson point processes for event counts. 483

VII.B.2 Independent and identically distributed (i.i.d.) events. 485

VII.B.3 Likelihood factorisation and conditional independence. 486

VII.C Violation of statistical independence. 489

VII.C.1 Detector effects. 490

VII.C.2 Pileup 492

VII.C.3 Unfolding and data processing. 495

VII.C.4 Global constraints. 499

VII.D Consequences for inference. 504

VII.E Formalism. 509

VII.F Uncertainty quantification. 523

VII.F.1 Analytic approaches: asymptotic theory and its limitations. 523

VII.F.2 Godambe information: the sandwich estimator) . . 527

VII.F.3 Wilks' theorem violations and Bartlett corrections . 531

VII.F.4 Numerical resampling approaches: bootstrapping and toy Monte Carlo. 536

VII.F.4.i Non-parametric bootstrap resampling. . . 537

VII.F.4.ii Parametric bootstrap: toy Monte Carlo simulations 544

VII.F.4.iii Practical considerations and guidelines. . 549

VII.F.4.iii.a Number of replicas. 549
VII.F.4.iii.b Computational cost and parallelisation. . . . 550
VII.F.4.iii.c Diagnostics for coverage and reliability. . . . 551
VII.F.4.iii.d Incorporating systematic uncertainties. . . . 552
VII.F.4.iii.e Reporting and using bootstrap results . . . 553
VII.F.4.iii.f Common pitfalls. 554
VII.G Case studies. 557
VII.G.1 Setup. 557
VII.G.2 Fully binned baseline 558
VII.G.2.i Methodology. 559
VII.G.3 Correlation diagnostics after unbinned unfolding . . 571
VII.G.3.i Pairwise weight–distance correlations . . . 574
VII.G.3.ii Histogram covariance matrices. 578
VII.G.3.iii Implications 579
VII.G.4 Unbinned unfolding: binned and unbinned inference. 581
VII.G.4.i Parameter bias 583

VII.G.4.ii Uncertainty estimation and coverage. 586

VII.G.5 Extension to higher dimensions. 594

VII.G.5.i Evaluation. 602

VII.H Conclusions and outlook. 607

VIII Symmetries in data: connections to unfolding challenges. 615

VIII.A Symmetries and unfolding. 616

VIII.A.1 The complementary nature of symmetry discovery and unfolding. 616

VIII.A.2 Symmetry aware cross sections. 620

VIII.B Formalism and Importance 629

VIII.B.1 Fundamental symmetries in HEP. 631

VIII.B.2 Symmetries in detector response functions 645

VIII.B.2.i Spatial uniformity and rotational symmetry. 645

VIII.B.2.ii Polar coverage and boost invariance. 647

VIII.B.2.iii Resolution effects and approximate invariance. 650

VIII.B.2.iv Mirror and charge symmetry. 652
VIII.B.2.v Permutation symmetry and identical particles. 654
VIII.B.3 How symmetries manifest in measured cross sections. 662
VIII.B.3.i Exact symmetries and flat distributions. . 663
VIII.B.3.ii Symmetries in kinematic shapes. 665
VIII.B.3.iii Interplay of physical and detector symmetries. 666
VIII.B.4 Challenges in identifying symmetries from noisy data. 668
VIII.B.4.i Dimensionality challenges. 671
VIII.C Statistical definition of dataset symmetries. 675
VIII.C.1 Distinction between point and dataset symmetries. 676
VIII.C.2 Inertial reference densities and their theoretical role 678
VIII.C.3 Inertial densities and relative symmetry. 681
VIII.C.3.i Failure of the naïve PDF preserving criterion. 682
VIII.C.3.ii Relative symmetry. 683
VIII.C.3.iii Choice of the inertial density. 684

VIII.C.4 Applications to particle physics. 685
VIII.D SymmetryGAN: Discovering Symmetries with Adversarial Learning 689
VIII.D.1 The SymmetryGAN Architecture 690
VIII.D.2 Machine Learning with Inertial Restrictions 692
VIII.D.3 Deep learning implementation details. 698
VIII.D.4 Verification. 700
VIII.D.5 Other symmetry discovery methods. 701
VIII.E Empirical experiments. 705
VIII.E.1 Gaussian experiments. 705
VIII.E.1.i One-dimensional Gaussian. 706
VIII.E.1.ii Two dimensional Gaussians. 708
VIII.E.1.iii Gaussian Mixture Models 713
VIII.E.2 Particle physics experiments. 718
VIII.E.3 Interpreting discovered symmetries. 728
VIII.F Towards symmetry inference. 730

VIII.G Symmetry informed unfolding 733
VIII.G.1 Symmetry preserving neural network architectures. 735
VIII.G.2 Reducing dimensionality through symmetry identification. 738
VIII.G.3 Hidden symmetries and emergent simplicity. 739
VIII.G.3.i Formalism 740
VIII.G.4 Applications for unfolding jet substructure variables. 743
VIII.H Improved precision using symmetries 745
VIII.H.1 Data augmentation using discovered symmetries. . 745
VIII.H.2 Symmetry constrained unfolding. 749
VIII.I Conclusion 752
VIII.I.1 Beyond linear symmetries. 752
VIII.I.2 Approximate symmetries and symmetry breaking. . 755
VIII.I.3 A unified framework. 757

IX Conclusion 759

IX.A Synthesis of Unfolding Methods 760

IX.B A Unified Framework for Modern Unfolding 765
IX.B.1 The Interplay of Physics and Learning 766
IX.B.2 Common Themes Across Methods 768
IX.C Advances in Cross Section Measurement 773
IX.C.1 Summary of Contributions 773
IX.C.2 Impact and Advances 776
IX.D Applications to Current and Future Experiments 781
IX.E Open Challenges and Future Directions 790
IX.E.1 Challenges in unfolding methodology 790
IX.E.2 Handling correlations in unbinned inference 791
IX.E.3 Background treatment in complex environments . . 792
IX.E.4 Systematic uncertainty propagation in ML methods 794
IX.E.5 Future Directions 795
IX.E.5.i Joint unbinned unfolding and nuisance parameter profiling 795

IX.E.5.ii Theoretical guarantees for ML-based unfolding 797
IX.E.6 Use on real experimental data 798
IX.F Closing: The Broader Vision 801

References **808**

List of Figures

I.1 η vs. y for various $^m/_{p_T}$ 6
I.2 A schematic illustration of the Standard Model [4]. 12

II.1 Coverage properties of Tikhonov regularisation and IBU . . . 101
II.2 Weight correlation between event pairs as a function of distance between events. 105

III.1 Neural network depth and width illustration 115
III.2 Shallow vs. deep NN 116
III.3 Forward pass 119

IV.1 2 bin example 263
IV.2 Gaussian example setup 265
IV.3 Gaussian unfolding results and posterior analysis 267
IV.4 Statistical calibration analysis for NPU and FBU 269
IV.5 Jet substructure unfolding results using NPU, FBU, and IBU . 271
IV.6 Corner plots for jet substructure observables 276

V.1 A schematic diagram of the training setup for Moment Unfolding. Like a GAN, g is the generator and d is the discriminator, but unlike a GAN g does not generate samples, it instead generates reweighting factors given by Equation (V.9). The reweighted Simulation dataset inherits its weight from the matching Generation dataset. The detector emulations are only run once, since a new simulated dataset is created via importance weights and not by changing the features themselves. 300
V.2 Effect of detector resolution on Truth and Generation datasets 324

V.3 (a) Distributions from the Gaussian example of particle level truth, generation, and reweighted generation i.e. Moment Unfolding. The agreement between the truth and reweighted samples demonstrates the qualitative performance of Moment Unfolding. (b) The weighted MLC loss from Equation (V.19) for fixed g but optimized d, found by scanning over β_1 and β_2. The correct value is indicated by a red star. Indicated in shaded blue is the 1σ bootstrapped interval for Moment Unfolding's prediction of β_a.The lower panel in each plot shows the ratio to truth. 326

V.4 Jet substructure distributions comparing truth, generation, and Moment Unfolding results 333

V.5 Loss landscapes showing Moment Unfolding parameter estimation accuracy for unfolding jet substructure variable. 334

V.6 Momentum dependent unfolding of inclusive jet substructure distributions 339

V.7 Momentum dependent differential moments of jet substructure observables . . . 340
V.8 Comparison of unfolding methods for momentum-dependent jet moments . . . 344

VI.1 Comparison of activation functions for neural network weight parametrisation . . . 433
VI.2 RAN architecture with generator and critic networks . . . 442
VI.3 Unfolding performance comparison between RAN and OmniFold under varying detector smearing . . . 466
VI.4 Unfolded particle level distributions for six jet substructure observables, comparing RAN, OmniFold, and IBU. . . . 468

VII.1 Detector and particle level distributions for the study on correlations during inference. . . . 560

VII.2 Characterisation of detector response effects through progressive smearing of Monte Carlo simulation. Panel (a) illustrates the impact of finite detector resolution on the observed distributions, showing how the Generation is broadened by convolution with Gaussian response functions of width σ_{det}. The total observed variance follows the quadrature sum $\sigma^2_{\text{observed}} = \sigma^2_{\text{particle}} + \sigma^2_{\text{det}}$. Panel (b) presents the corresponding binned response matrices $R(x_i \mid z_j)$, which encode the probability of bin migration due to detector effects. For perfect resolution ($\sigma_{\text{det}} = 0$), the response matrix is diagonal, indicating no bin migration. As detector resolution degrades, off diagonal elements become increasingly prominent, quantifying the probability of events generated in bin j being reconstructed in neighbouring bins. 561

VII.3 Comparison of uncertainty estimation methods for binned unfolded distribution parameters as a function of detector resolution. 566

VII.4 Validation of unbiased parameter extraction from unfolded distributions across varying detector resolutions. 567
VII.5 Event wise weight correlations as a function of separation distance for different unfolding methods. 573
VII.6 Covariance structure of binned unfolded distributions for KDE and NN-based methods. 580
VII.7 Comparison between binned and unbinned parameter inference with unbinned and binned unfolding methods as a function of detector resolution. 584
VII.8 Validation of asymptotic uncertainty estimates across dimensionalities in unbinned unfolding. 603
VII.9 Impact of detector resolution on asymptotic uncertainty reliability in 6-dimensional unfolding. 606

VIII.1 Architectural comparison of standard GAN and SymmetryGAN for automated symmetry discovery. 693

VIII.2 Analytic loss landscape for the one-dimensional uniform distribution $\mathcal{N}((0.5, 1))$ under affine transformations $g(x) = b + cx$. The landscape exhibits two distinct maxima (indicated by stars) corresponding to the identity transformation $(b, c) = (0, 1)$ and reflection $(b, c) = (1, -1)$, separated by a deep valley at $c = 0$. This topological barrier creates a disconnected solution space that deterministically routes optimisation trajectories based on initial parameter values. 707

VIII.3 Empirical validation of SymmetryGAN on 1 dimensional Gaussian data showing convergence to discrete symmetries based on initial conditions. 709

VIII.4 Loss landscapes demonstrating SymmetryGAN's ability to discover continuous $SO(2)$ and discrete V_4 symmetries in isotropic and anisotropic 2D Gaussians. 711

VIII.5 Controlled discretization of continuous $SO(2)$ symmetry into cyclic subgroups $\mathbb{Z}_q$ via constraint enforcement. 712

VIII.6 Orthogonal slices of $\mathrm{Aff}_2(\mathbb{R})$ symmetries for isotropic Gaussian. 714

VIII.7 Discrete symmetry structure of anisotropic Gaussian in $\mathrm{Aff}_2(\mathbb{R})$ discovered by SymmetryGAN. 715

VIII.8 SymmetryGAN's predictions for a bimodal Gaussian mixture with $\mathbb{Z}_2$ reflection symmetry and corresponding loss landscape validation. 716

VIII.9 Discovery of dihedral symmetries D_8 and D_4 in octagonal and square lattice Gaussian mixtures. 717

VIII.10 Symmetry discovery on transverse momenta of dijet events using SymmetryGAN with a $SO(2) \times SO(2)$ search space, where each jet undergoes independent azimuthal rotation $g_{\theta_1,\theta_2}(\mathbf{p}) = (R(\theta_1)\mathbf{p}_1, R(\theta_2)\mathbf{p}_2)$. (a) Distribution of converged parameters (θ_1^f, θ_2^f) from independent training runs initialised uniformly in $[0, 2\pi)^2$. The discovered symmetries cluster along the diagonal $\theta_1 = \theta_2$ (blue line), confirming that only simultaneous rotations preserve the dijet distribution, a direct consequence of transverse momentum conservation. (b) Symmetry discovery map $\Omega : (\theta_1^i, \theta_2^i) \mapsto \theta^f$ revealing the loss landscape dynamics. The final rotation angle follows $\theta^f = \frac{\theta_1^i+\theta_2^i}{2}$ when $|\theta_1^i - \theta_2^i| < \pi$ (shown in green), and $\theta^f = \frac{\theta_1^i+\theta_2^i}{2} - \pi$ when $|\theta_1^i - \theta_2^i| > \pi$ (shown in blue). This bisection rule represents the path of steepest ascent in the loss landscape, demonstrating how gradient dynamics naturally discover the physical constraint without prior knowledge. . . . 720

VIII.11 Visual validation of discovered dijet symmetry through transverse momentum preservation. 723
VIII.12 Non-uniform azimuthal distributions from random $SO(4)$ rotations demonstrating symmetry violation, and uniform azimuthal distributions from discovered symmetry confirming invariance of dijet system. 724
VIII.13 Kullback-Leibler divergence analysis showing discovered symmetries approach statistical noise floor. 726

VIII.14 Discriminator loss distributions validating discovered symmetries against theoretical optimum. The histogram shows *post hoc* discriminator losses when trained to distinguish original from transformed dijet events. Discovered symmetries (blue) achieve losses tightly clustered around $2 \log 2 \approx 1.386$ (dashed line), the theoretical minimum for perfect symmetries where transformed and original distributions are indistinguishable. Random $SO(4)$ rotations (black) yield significantly lower losses, indicating the discriminator easily identifies these as non-symmetries. The discovered transformations achieve losses within 1% of the theoretical optimum, providing independent confirmation that SymmetryGAN identifies genuine invariances of the dijet system without prior physics knowledge. 727

List of Tables

I.1 Unit conversions in natural units 3

II.1 Comparing the MC dependence and uncertainty propagation of traditional unfolding methods. 77

II.2 Distributional distance metrics for unfolding evaluation 97

IV.1 Computational cost comparison between FBU and NPU . . . 268

V.1 Summary of training hyperparameters used in the model. These values control the architecture, optimization behaviour, and regularization of the training process. 317

V.2 Moments of jet observables at particle level. First and second moments of m, q, w and z_g are shown for truth (HERWIG), generation (PYTHIA) and MOMENT UNFOLDING. Uncertainties in the truth and generation columns are estimated via bootstrap resampling; uncertainties in the unfolding column combine in quadrature the generation bootstrap uncertainty with the empirical 1σ spread from repeated unfolding on the same dataset. 331

VI.1 Comparison of measurement approaches. Reporting only low–order moments loses most distribution information. Binned differential cross sections retain shape information but suffer from discretization and limited dimensionality. Full spectral measurements preserve the complete distribution, enabling maximal reusability and detailed theory comparisons, but require regularizing a much more ill–posed training. 360

VI.2 Comparison of unfolding method characteristics 379

VI.3 Wasserstein distances between unfolded and true distributions 472

VI.4 VLC divergence between unfolded and true distributions . . . 473

VII.1 Sources of correlated uncertainties in cross section measurements 508

VII.2 Gaussian model parameters for multidimensional unfolding validation studies. 596

VIII.1 Comparative analysis of unfolding and symmetry discovery methods in particle physics. 621

VIII.2 Fundamental symmetries and their manifestations in HEP observables. 638

VIII.3 Symmetry breaking induced by detector effects in HEP experiments. 658

IX.1 Applications of methods to experimental scenarios 783

Chapter I

Introduction and physics background.

I.A Units and conventions.

Even though nature does not establish preferred units, the physics that describes it requires establishing a common language and framework. In high energy physics, the choice of units reflects a not simply an arbitrary choice, but a philosophical stance about the nature of reality. While everyday experience suggests that meters, kilograms, and seconds might be the most suitable units to express the physical world, particle physics reveals that speed, action, and energy form more natural rulers for measuring the universe at its smallest scales.

Definition I.1. *Natural Units* are a system where $\hbar = c = 1$, effectively setting the speed of light and quantum of action as fundamental measuring sticks. This choice transforms all physical quantities into powers of energy.

Some common physical quantities, their abbreviated natural units, their full natural units, their approximate SI equivalents and their physical significance are described in Table I.1.

Table I.1: Combined unit conversions in natural units, showing both abbreviated and full natural unit expressions, their SI equivalents and their physical significance.

Quantity	Abbrev.	Full unit	SI (approx.)	Comment
Speed	1	c	$3 \times 10^{8}\,\mathrm{m\,s^{-1}}$	Speed of light
Action	1	$\hbar$	$10^{-34}\,\mathrm{J\,s}$	Quantum of action
Energy	GeV	GeV	$1.6 \times 10^{-10}\,\mathrm{J}$	Binding energy
Momentum	GeV	GeV/c	$5.3 \times 10^{-19}\,\mathrm{N\,s}$	Typical HEP particle momentum
Mass	GeV	GeV/c^2	$1.8 \times 10^{-27}\,\mathrm{kg}$	Proton mass
Length	GeV^{-1}	$\hbar c/\mathrm{GeV}$	$2 \times 10^{-16}\,\mathrm{m}$	Compton wavelength
Time	GeV^{-1}	$\hbar/\mathrm{GeV}$	$6.6 \times 10^{-25}\,\mathrm{s}$	
Charge	1	$e/\sqrt{4\pi\alpha}$	$5.3 \times 10^{-19}\,\mathrm{C}$	$\mathrm{e} = 1.6 \times 10^{-19}\,\mathrm{C} \approx 0.3$
Cross section	GeV^{-2}	$\hbar^2 c^2/\mathrm{GeV}^2$	$4 \times 10^{-32}\,\mathrm{m}^{-2}$	barn=$2.6 \times 10^{-9}\,\mathrm{GeV}^{-2}$
$\boldsymbol{B}$ field	GeV^2	$\mathrm{GeV}^2/\hbar c^2$	$5 \times 10^{16}\,\mathrm{T}$	

I.A.1 Coordinate systems and relativistic geometry.

At a high energy physics (HEP) experiment, the choice of coordinates must respect the underlying symmetries of the physics and the experimental setup. The laboratory frame typically provides a natural Cartesian system. For example, for a circular collider experiment, one can set the z–axis to be along the beam direction (longitudinal), the x–axis to be horizontal, pointing toward the centre of the accelerator ring and the y–axis to be vertical, completing the right handed system.

However, the partons that participate in an interaction can carry unknown fractions of the beam momentum, making the centre of mass frame of each interaction unknowable. This uncertainty motivates a coordinate system that transforms simply under longitudinal Lorentz boosts.

Definition I.2. The *pseudorapidity* η, is defined as

$$\eta = -\ln\tan\frac{\theta}{2} \tag{I.1}$$

where θ is the polar angle from the beam axis [1]. Under a longitudinal boost with rapidity $\beta = \operatorname{artanh} {}^{v}\!/_{c}$, a massless particle's η transforms as $\eta \mapsto \eta + \beta$

Expressing θ in terms of momentum,

$$\eta = -\ln\tan\frac{\theta}{2} = \frac{1}{2}\ln\frac{|p| + p_z}{|p| - p_z} = \operatorname{artanh}\frac{p_z}{|p|} \tag{I.2}$$

Figure I.1 shows the relationship between pseudorapidity η and true rapidity y for particles with different mass to p_T ratios. As expected, the massless case $(m/p_T = 0)$ lies exactly on the diagonal $y = \eta$, while non-zero ${}^{m}/{}_{p_T}$ introduces a systematic deviation that grows at large $|\eta|$. Even a modest ratio $(m/p_T = 0.1)$ produces a measurable shift, and by $m/p_T = 2.0$ the rapidity is significantly reduced relative to η. This behaviour must be accounted for when inferring kinematic distributions of heavy particles from detector measurements expressed in pseudorapidity.

For massless particles, differences in η remain invariant under longitudinal boosts, motivating the definition of the angular distance as follows.

Definition I.3. The *angular distance metric* is defined as

$$\Delta R^2 = \Delta\eta^2 + \Delta\varphi^2, \tag{I.3}$$

where φ is the azimuthal angle around the beam axis. This metric approximates the geometric angle between particles in the detector while remaining approximately boost invariant.

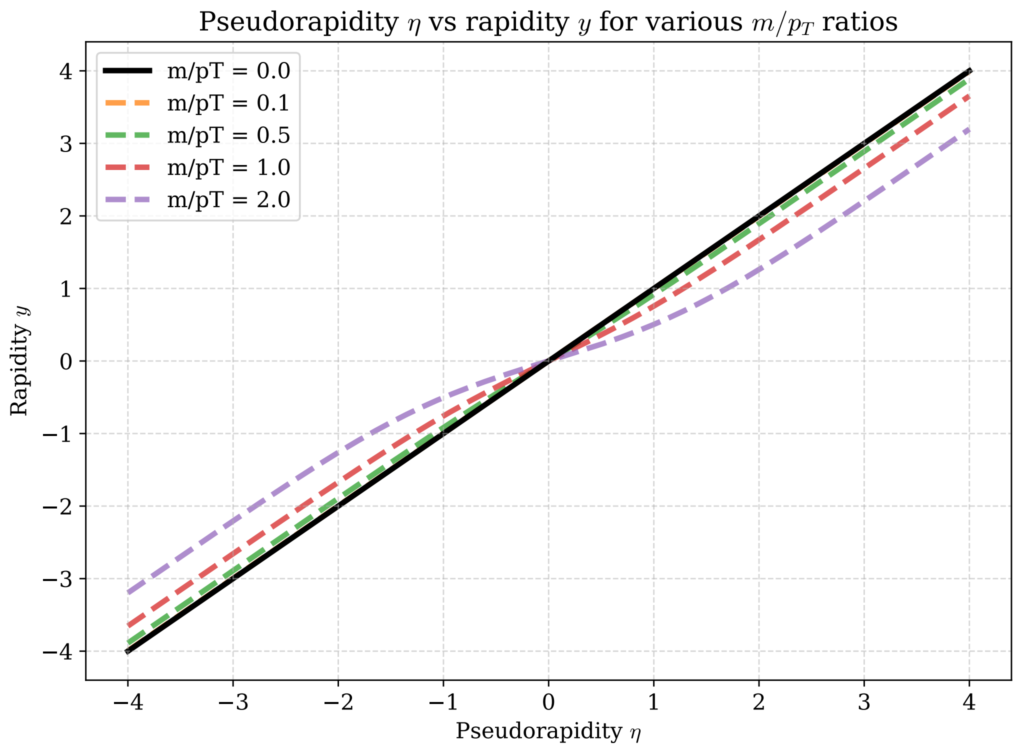

Figure I.1: Comparison of pseudorapidity η and true rapidity $y = \frac{1}{2}\ln\frac{E+p_z}{E-p_z}$ for several mass to transverse momentum ratios. Curves correspond to $^{m}/_{p_T} = 0.0,\ 0.1,\ 0.5,\ 1.0,\ 2.0$, illustrating how finite mass distorts away from the massless limit $y = \eta$ at large $|\eta|$.

I.A.2 Statistical frameworks and uncertainty quantification.

In modern particle physics analyses, every measurement emerges from millions of interaction events, each carrying both statistical and systematic uncertainties.

Definition I.4. The *Poisson distribution* is the fundamental distribution governing counting experiments. For n observed events with expected value λ,

$$\mathbb{P}(n \mid \lambda) = \frac{\lambda^n e^{-\lambda}}{n!} \tag{I.4}$$

In the high statistics limit, $(n \to \infty)$, the Poisson distribution approaches a Gaussian.

Definition I.5. The *profile likelihood ratio*

$$\mathcal{L}(\mu) = \frac{L(\mu, \hat{\theta}_\mu)}{L(\hat{\mu}, \hat{\theta})} \tag{I.5}$$

where $\hat{\theta}_\mu$ maximises L for fixed signal strength μ is the optimal test statistics for hypothesis testing under the Neyman–Pearson lemma.

I.A.3 Machine learning architectures and notation.

Neural networks can be specified by their architecture vectors, $[d_0, d_1, \ldots, d_\ell]$, which denotes a network with input dimension d_0, hidden layers of dimensions d_1 through $d_{\ell-1}$, and output dimension d_ℓ.

For a network $f : \mathbb{R}^{d_0} \to \mathbb{R}^{d_\ell}$ with parameters $\theta = \{W_i, b_i\}$, the forward pass computes

$$h_0 = x \tag{I.6}$$

$$h_i = \sigma(W_i\, h_{i-i} + b_i) \quad i = 1, \ldots, \ell - 1 \tag{I.7}$$

$$f(x;\theta) = W_\ell\, h_{\ell-1} + b_\ell \tag{I.8}$$

where σ denotes the activation function. The universality theorem guarantees that sufficiently wide networks can approximate any continuous function.

Training proceeds via gradient descent on a loss function $L(\theta)$, with the gradient computed through automatic differentiation.

I.A.4 Information theory and optimal observables.

Information theory provides a rigorous framework through the Neyman-Pearson lemma, which implies that the likelihood ratio $\frac{L(x|S)}{L(x|B)}$ provides the most powerful test for distinguishing signal S from background B at any given significance level.

In practice, this optimal observable can be approximated using machine learning classifiers. A well trained classifier computes

$$f(x) \approx \mathbb{P}(S|x) = \frac{L(x \mid S)\,\mathbb{P}(S)}{L(x \mid S)\,\mathbb{P}(S) + L(x \mid B)\,\mathbb{P}(B)]} \tag{I.9}$$

The mutual information $I(Y; f(X))$ between the true labels Y and classifier output $f(X)$ quantifies the information captured

$$I(Y; f(X)) = \iint p(y, f)\; \log \frac{p(y, f)}{p(y)\,p(f)} \mathrm{d}y\, \mathrm{d}f. \tag{I.10}$$

This connects directly to the area under the ROC curve and provides a model-independent measure of classification performance.

I.A.5 A note on conventions and clarity.

This work strives to maintain a balance between mathematical rigour and physical insight. Where conventions differ between communities,[1] attempts are made to note both conventions.

[1]For example, particle physicists and machine learning researchers.

I.B The Standard Model: Theoretical framework.

The Standard Model of particle physics represents one of the most significant intellectual achievements in modern science. Developed throughout the latter half of the 20^{th} century, it provides a quantum field theory framework that describes three of the four known fundamental forces—the electromagnetic, weak, and strong interactions—in addition to classifying all known elementary particles. The mathematical formulation of the Standard Model is based on gauge theory, specifically quantum chromodynamics (QCD) and the electroweak theory, underpinned by the gauge symmetry group $SU(3)_C \times SU(2)_L \times U(1)_Y$.

The predictive power of the Standard Model has been repeatedly validated through precision experiments across multiple energy scales, from low energy nuclear phenomena to the highest energy particle collisions achievable at modern accelerators. Its crowning achievement came with the discovery of the

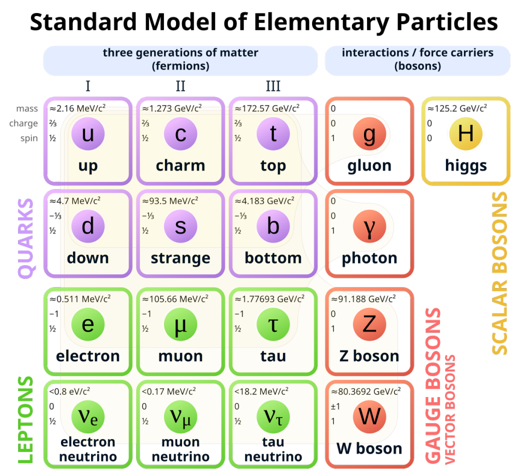

Figure I.2: A schematic illustration of the Standard Model [4].

Higgs boson in 2012 at the Large Hadron Collider (LHC) [2, 3], confirming the mechanism through which elementary particles acquire mass. A schematic illustration of the standard model can be found in Figure I.2.

I.B.1 Fundamental particles and forces.

The Standard Model categorises elementary particles into two main families: fermions, which comprise matter, and bosons, which mediate forces between matter particles.

I.B.1.i Fermions: The building blocks of matter.

Fermions, characterized by half–integer spin, obey the Pauli exclusion principle and satisfy Fermi–Dirac statistics. Fermions are further classified into quarks and leptons, each arranged in three generations of increasing mass.

I.B.1.i.a Quarks.

Quarks are spin = $^1/_2$ particles that are catagorised into three generations as follows:

- Up (u) and down (d),
- Charm (c) and strange (s),

- Top (t) and bottom (b).

Quarks carry fractional electric charge and colour charge, and experience all fundamental forces. They are confined within hadrons—composite particles categorized as baryons[2] or mesons[3].

I.B.1.i.b Leptons.

Like quarks, leptons too are spin ½ particles that are catagorised into three generations.

- Electron (e) and electron neutrino (ν_e),
- Muon (μ) and muon neutrino (ν_μ),
- Tau (τ) and tau neutrino (ν_τ).

Electrons, muons, and taus carry unit electric charge and interact through the electromagnetic and weak forces, while neutrinos are electrically neutral

[2] three quark states, like protons and neutrons.
[3] quark–antiquark pairs.

and interact only through the weak force, making them notoriously difficult to detect.

I.B.1.ii Bosons: Force carriers.

Bosons, with integer spin values, mediate the fundamental interactions. They are not subject to the Pauli exclusion principle and instead satisfy Bose–Einstein statistics. The Standard Model comprises the following bosons:

- The photons (γ), is a massless spin–1 boson that mediates the electromagnetic force,
- $W^{\pm}$ and Z bosons are massive spin–1 bosons that mediate the weak force,
- Gluons (g) are a set of eight massless spin–1 bosons that mediate the strong force, and
- the Higgs boson (H) is a massive spin–0 boson associated with the Higgs field that gives mass to elementary particles

I.B.2 Theoretical framework and symmetries.

The Standard Model is constructed through principles of quantum field theory where particles are excitations of underlying quantum fields. Its mathematical structure is determined by local gauge invariance under the following specific symmetry transformations:

- $U(1)_Y$ is associated with electroweak hypercharge and is the symmetry of electroweak theory,
- $SU(2)_L$ describes the weak isospin, and acts on left-handed fermions, and
- $SU(3)_C$ governs the strong interactions through color charge in QCD.

Electroweak unification, demonstrated by Glashow [5], Weinberg [6], and Salam [7], demonstrates how the electromagnetic and weak forces emerge as different aspects of a single electroweak interaction, which undergoes spontaneous symmetry breaking at low energies.

I.B.3 The Higgs mechanism and mass generation.

The Higgs mechanism, proposed by Peter Higgs in the 1960s [8], addresses the theoretical inconsistency of massive gauge bosons in a gauge invariant theory. The mechanism introduces a scalar field—the Higgs field—that permeates space and spontaneously broke the electroweak symmetry when the universe cooled after the Big Bang.

This symmetry breaking generates masses for the W and Z bosons while leaving the photon massless, explaining the significant difference between the electromagnetic and weak forces at ordinary energies. Additionally, the Higgs field couples to fermions through Yukawa interactions [9], generating their masses with coupling strengths proportional to the particle masses.

The discovery of the Higgs boson at the LHC in 2012, with properties consistent with Standard Model predictions, provided crucial experimental validation of this mechanism and completed the Standard Model's particle roster.

I.B.4 Limitations and beyond the Standard Model (BSM) physics.

Despite its remarkable success, the Standard Model has several well recognised limitations, including,

1. It does not incorporate gravity, the fourth fundamental force.
2. It fails to explain the observed matter–antimatter asymmetry in the universe.
3. It does not account for dark matter or dark energy, which together constitute about 95% of the universe's energy content.
4. It requires fine tuning of parameters, raising theoretical concerns like the hierarchy problem.
5. It does not explain neutrino masses, which must exist given observed neutrino oscillations.

These limitations motivate theoretical extensions and experimental searches for physics beyond the Standard Model, including supersymmetry, grand unified theories, and various dark matter candidates. Precision measurements at particle physics experiments provide one of the most powerful approaches to probe these potential extensions, making analysis techniques like those discussed in this thesis essential for advancing our fundamental understanding of nature.

I.C Fundamental role of cross section measurements in particle physics.

Differential cross section measurements are the fundamental currency of scientific exchange in particle physics, serving as the primary bridge between theoretical predictions and experimental observations. These measurements quantify the probability density of specific particle interactions as a function of kinematic variables, providing the essential link between theoretical predictions and experimental observations. A cross section quantifies the probability of a specific particle interaction occurring and is typically expressed in units of area (barns, where 1 barn = 10^{-24}cm^2). This seemingly simple concept forms the cornerstone of how we test and validate our understanding of fundamental physics.

The Standard Model makes precise predictions for cross sections that can be directly tested at particle physics experiments. Any statistically significant deviation between measured cross sections and theoretical predictions may signal the presence of new physics beyond the Standard Model [10].[4]

Cross sections are particularly powerful because they encode the underlying quantum field theory structure in a form that can be directly probed by experiment. For instance, measurements of jet production cross sections at different energy scales reveal the running of the strong coupling constant α_S [11], while precision electroweak cross section measurements constrain the properties of the Higgs boson and other fundamental particles [12]. In searches for physics beyond the Standard Model, differential cross section measurements can reveal subtle deviations that point to new particles or interactions, even when direct observation is beyond experimental reach.

These measurements also serve a crucial role in constraining effective field theories (EFTs) that parameterise potential new physics in a model independent way. By measuring differential distributions with high precision,

[4]Such deviations might also signal errors in the theoretical framework used for predictions or in the experimental procedures used to measure the cross section.

experiments can place bounds on EFT coefficients, narrowing the space of viable theoretical extensions to the Standard Model [13].

For example, the ongoing precision program at the Large Hadron Collider (LHC) relies heavily on refined cross section measurements to extract maximum physical insight from collected data. In addition to driving comparisons with theoretical models, cross section measurements are also used at high energy physics experiments for MC tuning [14] and consistency checks [15] among other applications.

I.D Cross section measurements: From theory to experiment.

I.D.1 Theory.

Classically, the cross section (σ) represents the effective area within which two particles must interact for a particular process to occur.

Definition I.6. For collisions between discrete particles, the *cross section* is defined as the area transverse to their relative motion. If the particles were to interact via contact forces (e.g., hard spheres), the cross section corresponds to their geometric size. For long range forces however, the cross section is larger than the physical dimensions of the particles due to action–at–a–distance effects.

Definition I.7. The *differential cross section* ($\frac{d\sigma}{d\Omega}$) provides additional granularity by describing how the probability of scattering depends on specific final state variables, such as scattering angle (θ) or energy transfer. It is defined as

$$\frac{\mathrm{d}\sigma}{\mathrm{d}\Omega} = \frac{\text{Number of events scattered into } \mathrm{d}\Omega}{\text{Incident flux} \times \text{Target density}}. \tag{I.11}$$

The total cross section can be recovered by integrating over solid angle:

$$\sigma = \int_{4\pi} \frac{\mathrm{d}\sigma}{\mathrm{d}\Omega}\, \mathrm{d}\Omega. \tag{I.12}$$

While the classical picture above is intuitive, scattering at HEP experiments is governed by quantum field theory (QFT). In this framework the probability for a process is encoded in a Lorentz invariant matrix element $\mathcal{M}$.

For a $2 \to n$ reaction with incoming 4−momenta $p_{1,2}$ and final state phase space $\mathrm{d}\Phi_n$, the fully differential cross section is

$$\mathrm{d}\sigma = \frac{(2\pi)^4\, \delta^{(4)}\big(p_1 + p_2 - \sum_{i=1}^{n} p_i\big)}{4\sqrt{(p_1 \cdot p_2)^2 - m_1^2 m_2^2}}\, |\mathcal{M}|^2\, \mathrm{d}\Phi_n, \tag{I.13}$$

where the denominator is the flux factor and $\mathrm{d}\Phi_n = \prod_{i=1}^{n} \frac{\mathrm{d}^3 p_i}{(2\pi)^3 2E_i}$ is the Lorentz invariant phase space element.[5] Equation (I.13) reduces to the classical area when $|\mathcal{M}|^2$ is replaced by a contact interaction and the final

[5]Standard derivations can be found in [16–19].

state integral collapses to a single kinematic configuration. Integrating Equation (I.13) over final state kinematics yields the total cross section, $\sigma = \int \mathrm{d}\sigma$.

At tree level, $|\mathcal{M}|^2$ is computed from Feynman rules derived from the Lagrangian, while higher order corrections incorporate loops, parton showers, and non-perturbative effects such as hadronisation. For practical experimental predictions predictions one folds $|\mathcal{M}|^2$ with parton distribution functions (PDFs) and convolves the result with detector response—precisely the forward process that the unfolding methods developed in this thesis seek to invert.

Differential cross sections have a long history of providing valuable insights for probing fundamental properties of particles and interactions. Their use dates all the way back to Rutherford's scattering experiments that revealed the existence of atomic nuclei by analysing angular distributions of scattered alpha particles [20].

I.D.2 Experimental Measurement

At modern colliders[6] the two beams themselves act as both "projectile" and "target." The basic experimental quantity is the instantaneous luminosity.

Definition I.8. The *luminosity* $\mathcal{L}(t)$ is defined such that the interaction rate for a process with cross section σ is $\mathrm{d}N/\mathrm{d}t = \mathcal{L}(t)\,\sigma$.

Time integrating over a data taking period $[t_0, t_f]$ yields the integrated luminosity.

Definition I.9. The *integrated luminosity* $\mathcal{L}_{\text{int}}$ is defined as

$$\mathcal{L}_{\text{int}} = \int_{t_0}^{t_f} \mathcal{L}(t)\,\mathrm{d}t, \qquad \sigma = \frac{N_{\text{obs}} - N_{\text{bkg}}}{\mathcal{L}_{\text{int}}\,\epsilon\,A}. \tag{I.14}$$

[6]This section focusses on collider experiments, but similar analyses can be applied to non-collider HEP experiments as well, such as fixed target experiments. [21] and chapters 31 to 38 of [10] provide a comprehensive and detailed exposition of experimental measurement in HEP. [22, 23] focus specifically on fixed target techniques and phenomenology. [24] compares collider and fixed target formalisms, reviews luminosity analogues, and details the role of detector simulations and unfolding in a fixed target context

Here N_{obs} is the number of selected events, N_{bkg} an estimate of background contaminations, ϵ the detector and selection efficiency and A the geometric–plus–kinematic acceptance of the analysis.

For binned measurements one bins events in an observable X[7] and divides by the bin width.

$$\left.\frac{\mathrm{d}\sigma}{\mathrm{d}X}\right|_{X_i} = \frac{1}{\mathcal{L}_{\text{int}}\,\Delta X_i}\frac{N_i^{\text{obs}} - N_i^{\text{bkg}}}{\epsilon_i\,A_i}, \tag{I.15}$$

with the index i denoting the i^{th} bin.

Luminosity determination is itself a precision measurement, usually performed with dedicated luminometers that exploit van der Meer scans or pileup counting techniques. The efficiency–acceptance term $\epsilon\,A$ is obtained from full detector simulations and corrected in data using control samples and "tag–and–probe" methods.

Equations (I.14) and (I.15) thus link the theoretically calculated parton level cross sections (*vide*Equation (I.13)) to the raw observables recorded by the a detector, completing the chain from theory to experiment.

[7]For example, transverse momentum p_T or rapidity y

I.D.3 Applications in particle physics.

As mentioned above, cross section measurements serve as the fundamental currency of particle physics, translating abstract theoretical predictions into measurable experimental quantities. However, their applications extend far beyond simple theory validation into the operational heart of how experiments function, analyse data, and cross–validate results.

I.D.3.i Theory validation.

As discussed above, comparing measured cross sections with predictions from quantum field theory validates and tests theoretical models like quantum chromodynamics and electroweak theory, by encapsulating interaction probabilities in a measurable form. Deviations from expected cross sections may indicate new phenomena, such as supersymmetric particles or dark matter candidates.

Differential cross sections also provide constraints on effective field theories and parton distribution functions (PDFs), essential for understanding the internal structure of hadrons. Unfolded cross section measurements allow comparisons with theoretical models years after data collection, even if detector simulations are no longer available, further enhancing their utility, and future proofing the data. Their determination requires careful design and analysis techniques to account for systematic uncertainties introduced by detector effects.

I.D.3.ii Monte Carlo tuning.

Definition I.10. *Monte Carlo tuning* is the iterative process of adjusting simulation parameters to match measured cross sections, ensuring that detector simulations accurately reproduce real experimental data.

Cross section measurements are extensively used in Monte Carlo (MC) tuning.

Every particle physics analysis relies on sophisticated simulations that model everything from the initial parton interactions through hadronisation to the detector response. These simulations contain dozens of phenomenological parameters, such as the strong coupling constant at various scales and non-perturbative fragmentation functions.

Definition I.11. *Parton distribution functions* (PDFs) are probability distributions that describe the probability of finding a parton (quark or gluon) in a hadron at a given momentum fraction x and scale Q^2. PDFs are determined from global fits to a wide range of hard scattering processes, including deep inelastic scattering, Drell–Yan production, and jet production.

Measured cross sections provide the ground truth that anchors these simulations to reality.

Consider the following example: When CMS measures the inclusive jet cross section at a new centre–of–mass energy, that measurement immediately becomes a crucial input for tuning generators like Pythia or Herwig. The differential distributions—whether in transverse momentum, rapidity, or invariant mass—reveal where the models succeed and where they fail. A discrepancy in the high$-p_T$ tail might indicate a need to adjust the modelling of initialstate radiation; unexpected structure in angular distributions could point to missing higher order QCD effects.

I.D.3.iii Consistency checks.

Cross–validations between different experimental approaches, detector configurations, or analysis methods ensure measurement reliability and identify systematic biases. Cross sections serve as essential tools for consistency checks across multiple dimensions of experimental physics. Within a single experiment, measuring the same process through different decay channels provides a powerful systematic cross check. For instance, measuring the W boson production cross section through both electronic and muonic decays tests the understanding of lepton universality while simultaneously validating detector calibrations. Any significant deviation signals either new physics, errors in the phenomenological method used, or unaccounted systematic effects.

Between experiments, cross section measurements enable crucial cross–experiment validation. When CMS and ATLAS measure the same process with independent detectors and analysis chains, agreement within uncertainties validates both measurements. Disagreement, conversely, can reveal subtle systematic effects or push calculations to higher precision.

These applications cascade through every level of experimental operations.

I.D.3.iv Luminosity determination.

Luminosity determination becomes possible through processes with well–known theoretical cross sections. Van der Meer scans calibrate the absolute luminosity scale, but elastic scattering and other standard candle processes provide continuous monitoring. The uncertainty on integrated luminosity, typically 2 to 3%, directly impacts every cross section measurement, creating a web of interdependencies.

I.D.3.v Background estimation.

Background estimation in searches for new physics relies on measured cross sections of Standard Model processes. When searching for supersymmetric particles, the irreducible backgrounds from $W+$ jets or $t\bar{t}$ production must be understood at the percent level. Control regions enriched in backgrounds, combined with precise cross section measurements, enable data driven background estimates that would be impossible from simulation alone.

I.D.3.vi Parton luminosity.

Definition I.12. *Parton luminosity* is the effective luminosity for specific parton–parton interactions, calculated by convolving the total luminosity with parton distribution functions.

A particularly elegant application of cross sections emerges in parton luminosity calculations. Since protons are composite objects, the effective luminosity for producing heavy particles depends on the convolution of PDFs with the partonic cross section. Measurements of Drell–Yan production at different invariant masses directly probe the quark and antiquark distributions, while inclusive jet production constrains the gluon PDF. This creates a self–consistent feedback loop, where better PDFs enable more precise predictions, which enable more sensitive measurements, which further constrain the PDFs.

I.D.3.vii Detector performance validation.

Detector performance validation represents another major application of cross section measurements. Measured cross sections for well understood processes serve as standard candles for monitoring detector stability over time. For example, slow drift in the measured $Z \to \mu\mu$ cross section might indicate degrading muon chamber performance long before it would be noticed in individual event displays. These measurements become part of the experiment's data quality monitoring, flagging problems in real time.

I.D.3.viii Systematic uncertainty evaluation.

The role of cross section measurements in systematic uncertainty evaluation cannot be overstated. Every measurement must account for theoretical uncertainties in signal and background processes. By measuring auxiliary cross sections, for instance, $Z+$ jets production when studying $W+$ jets, experiments can constrain these uncertainties using data rather than relying solely on theoretical estimates. This *in situ* constraint often reduces systematic uncertainties by factors of two or more.

I.D.3.ix Future planning.

Finally, cross sections enable physics program planning for future experiments. The measured production rates at current energies, extrapolated using theoretical calculations, determine required luminosities and detector capabilities for next–generation experiments. For exmaple, the surprisingly large Higgs production cross section at the LHC, for instance, has already influenced design considerations for future electron–positron Higgs factories.

1em In sum, cross sections certainly do function as the Rosetta Stone of particle physics, translating between the languages of theory, simulation, and experimental measurement while maintaining coherence across all three domains. However, they serve not merely as endpoints of analyses, but as the connective tissue that binds together theory, simulation, and experiment into a coherent whole. They simultaneously test theoretical understanding, calibrate experimental tools, and point the way toward new discoveries. This multiplicative utility explains why cross section measurements, even of well studied processes, remain at the heart of every particle physics experiment.

I.E Detector response in precision measurements.

The direct comparison between theoretical predictions and experimental measurements is complicated by detector effects. HEP detectors are technological marvels that capture the trajectories of charged particles, energy deposits in calorimeters, and timing and pattern–recognition information from tracking and particle–identification systems, but they introduce distortions that must be carefully accounted for to extract the true physical distributions of interest. Particle physics detectors represent some of humanity's most sophisticated sensing apparatūs——capturing particle trajectories with silicon sensors operating at liquid helium temperatures, measuring energy deposits in dense calorimeter crystals, and reconstructing vertices with sub–millimetre precision. Yet these technological marvels inevitably introduce systematic distortions that transform the pristine theoretical predictions into the messy reality of experimental data.

Consider the information degradation that occurs in every measurement. Finite resolution creates fundamental blurring, much like how a camera lens distorts an image. The detector's discrete sensing elements can only measure particle energies, momenta, and positions to finite precision, creating an inherent convolution between the true physics distribution and the instrument response function. Geometric acceptance imposes hard boundaries on observable phase space. Particles scattered into the forward beam pipe or extreme backward angles simply vanish from the recorded dataset, creating holes in the measurement that no amount of statistics can fill.

Detection efficiency varies across the detector's active volume, introducing a complex weighting function that depends on particle type, energy, and trajectory. A high–energy muon might traverse the entire detector with near–perfect efficiency, while a low–energy hadron could be absorbed in the first layers of material. Particle misidentification compounds these challenges through cross–contamination between categories, such as when hadronic shower fluctuations cause a pion to masquerade as a kaon [25].

In this way every detector measurement embeds two irreducible probability relationships.

1. Detection incompleteness: $p(\text{measured}|\text{true}) < 1$ True events that fail to be recorded

2. Measurement impurity: $p(\text{true}|\text{neasured}) < 1$ Recorded events that represent contamination

This reveals why detector corrections are fundamentally different from simple calibrations. Unlike adjusting a scale that consistently reads, say, 5% high, detector response involves dual information loss that operates asymmetrically.

The first inequality captures the selection bias where certain true configurations have zero probability of detection, creating null spaces in the measurement. The second inequality captures the contamination bias where every reconstruction category contains some fraction of misclassified events.

Background contamination represents a third problem—every measurement category contains some admixture of misclassified events. When hadrons interact in electromagnetic calorimeters, they can mimic electron signatures. When cosmic ray muons traverse the detector during a collision, they contribute to the muon count despite having no connection to the physics of interest. This contamination creates what in signal processing is called the false positive rate.

The mathematical relationship between true particle level distributions and observed detector level measurements follows the convolution integral

$$p(x) = \int r(x|z)\, p(z)\, \mathrm{d}z \tag{I.16}$$

Where $p(x)$ is the detector level density, $p(z)$ is the particle level density and $r(x|z)$ serves as the response kernel, the conditional probability density that maps each possible true configuration z to the distribution of possible detector measurements x. This kernel encapsulates the entire cascade of finite resolution information degradation.

The response kernel is analogous to the optical transfer function in image processing. It describes how the "lens" of the detector blurs and distorts the perfect theoretical "image". The response function inherently embeds both probabilistic asymmetries. Regions where $\int r(x|z)\ \mathrm{d}x < 1$ reveal acceptance holes, i.e. true configurations that produce no detector signal whatsoever. Conversely, the convolution structure itself ensures that multiple truth distributions can yield identical detector observations, creating the degeneracy problem that makes direct inversion impossible.

A central challenge then, for particle physics, is inverting this response kernel to recover $p(z)$ from observed data $p(x)$. This inversion is mathematically ill–posed precisely because of the information loss. Standard matrix inversion fails catastrophically, amplifying statistical noise into wild oscillations that bear no resemblance to the underlying physics.

The resolution requires sophisticated regularisation methods that impose additional constraints such as smoothness assumptions, positivity requirements, and prior knowledge about the expected signal shape. These constraints transform the ill–posed inverse problem into a well defined statistical inference challenge, though at the cost of introducing systematic uncertainties that must themselves be carefully validated.

The detector response problem exemplifies a universal pattern in experimental science: the tension between instrumental precision and information preservation. From astronomical imaging through medical diagnosis to HEP measurements, the fundamental trade off between sensitivity and purity governs all attempts to extract signal from noise.

I.F Challenges at modern experiments.

Several challenges at the modern HEP experiments make cross section measurements particularly demanding.

- **High dimensional phase spaces**: Modern measurements often involve multiple correlated observables, creating high dimensional distributions that are difficult to analyse with traditional methods.

- **Limited statistics in extreme regions**: Rare processes or the tails of distributions often contain valuable physics information but suffer from limited statistics.

- **Complex detector effects**: Detectors have non-trivial response functions that can vary significantly across phase space, and are only known implicitly through precision simulations. Their explicit functional form is unknown.

- **Theoretical uncertainties**: Precision measurements are increasingly limited by theoretical uncertainties in both signal and background modelling.

- **Computational constraints**: Detailed simulation of detector response requires substantial computing resources, limiting the statistical precision of response modeling.

These challenges make the unfolding problem increasingly difficult, particularly as measurements probe more complex final states and differential distributions. For example, measurements of jet substructure, which probe the detailed radiation pattern within collimated sprays of particles, involve observables with complex correlations and detector effects that vary based on jet energy, rapidity, and substructure properties themselves [26–28].

The need for unfolding arises from the fundamental requirement to present results in a detector independent form that can be directly compared with theory predictions or results from different experiments. Without this correction, theoretical interpretations would need to incorporate experiment specific detector simulations, significantly complicating scientific exchange and theoretical analysis, and inter–experiment comparisons would simply not be possible.

I.G Thesis Scope and Physics Impact

This dissertation focuses on developing, analysing, and applying novel machine learning methods for cross section measurements in particle physics, with particular emphasis on unbinned approaches that overcome limitations of traditional techniques. The work spans the spectrum from improving binned methods with neural posterior estimation to completely unbinned approaches for both full distributions and statistical moments.

The primary contributions of this thesis include:

1. Development of Neural Posterior Unfolding (NPU), enhancing binned approaches through normalising flows and amortised inference.

2. Introduction of Moment Unfolding, directly deconvolving distribution moments without binning.

3. Creation of Reweighting Adversarial Networks (RAN), a general framework for unbinned spectrum unfolding.

4. Analysis of event correlations in unfolded data and their impact on uncertainty estimation.

5. Investigation of symmetry discovery with SymmetryGAN and its connections to measurement constraints.

These methodological advances address fundamental challenges in experimental particle physics, potentially enhancing the precision and scope of measurements at present and future HEP experiments. These methods can have a wide range of applications in particle physics, including:

- Improved precision in jet substructure measurements, enabling better discrimination between different theoretical models of QCD radiation.

- Enhanced sensitivity to effective field theory parameters by directly deconvolving distribution moments.

- More robust uncertainty quantification in high dimensional measurements.

- Computational efficiency gains allowing for more detailed systematic studies.
- A rigorous statistical framework for incorporating detector response uncertainties in the unfolding process.

By bridging sophisticated machine learning techniques with the specific requirements of particle physics measurements, this work aims to advance the ability to extract fundamental physical insights from complex experimental data. The methods developed here have applications beyond particle physics, potentially benefiting any field where deconvolution of instrumental effects is necessary for scientific inference.

Chapter II

Theoretical foundations.

II.A Statistical formulation of the unfolding problem.

Unfolding, also known as deconvolution, is the process of correcting detector distortions in experimental data to recover the true particle level distributions. This procedure is critical for comparing experimental results with theoretical predictions and for enabling detector independent analyses. The unfolding problem is inherently statistical and presents unique challenges due to its ill posed nature.

II.A.1 The detector response and forward problem.

The relationship between the particle level truth distribution $p(z)$ and the detector level measured distribution $p(x)$ is governed by the detector response function $r(x \mid z)$, which encapsulates the resolution effects.[1] Equation (I.16) describes the **forward problem**, where the true distribution $p(z)$ is mapped

[1]Efficiency and acceptance effects can also be incorporated if "empty" events are allowed.

to the measured distribution $p(x)$. The detector response function $r(x \mid z)$ can often be estimated through detailed simulations.

II.A.2 The inverse problem: Unfolding.

The goal of unfolding is to invert the forward problem and estimate the Truth, $p(z)$ from Data $p(x)$. Mathematically, this requires solving

$$p(z) = \int r^{-1}(z|x)\, p_{\text{measured}}(x)\, \mathrm{d}x, \tag{II.1}$$

where $r^{-1}(z|x)$ represents the inverse response kernel. However, this inversion is ill posed because small fluctuations in $p(x)$ can lead to large variations in $p(z)$ [29]. Regularisation techniques are therefore essential to stabilise the solution.

II.A.3 Likelihood based formulation.

In practice, unfolding is performed using statistical inference methods. Given a set of measured data $\mathbf{X}_{i=1}^{N}$, the likelihood function for a proposed truth distribution $p(z;\theta)$, parametrised by θ, is

$$\mathcal{L}(\theta;\mathbf{X}) = \prod_{i=1}^{N} p(x_i;\ \theta), \tag{II.2}$$

where

$$p(x;\ \theta) = \int r(x \mid z)\, p(x;\ \theta)\, \mathrm{d}z. \tag{II.3}$$

Maximising this likelihood yields an estimate of the parameters θ, which define the unfolded truth distribution. Regularisation can be incorporated into this framework by adding penalty terms to the likelihood or by constraining the parameter space.

II.A.4 Regularisation techniques.

Regularisation mitigates the instability of unfolding by imposing constraints on the solution. Common approaches include Tikhonov Regularization [30], in which one adds a penalty term proportional to the norm of the second derivative of $p(z)$, enforcing smoothness, and iterative methods which gradually refine estimates of $p(z)$, regularising by stopping before convergence.

These techniques balance fidelity to the measured data (prior independence) with stability of the unfolded solution.

II.A.5 Challenges in high dimensional phase spaces.

II.A.5.i Binned methods.

A significant challenge that traditional unfolding methods face is the *curse of dimensionality*. As the number of measured observables increases, the statistical power required to populate discrete bins grows exponentially, quickly overwhelming even the largest datasets collected at modern experiments.

Consider a measurement involving just four kinematic variables, say, transverse momentum, pseudorapidity, azimuthal angle, and invariant mass. With a modest 20 bins per dimension, the resulting joint histogram requires 1.6×10^5 bins. Most of these bins will contain zero events, creating a sparse matrix that renders traditional unfolding techniques numerically unstable.

[Scaling of relative uncertainty] Consider a d-dimensional measurement space partitioned into histogram bins of widths $\Delta z_1, \ldots, \Delta z_d$, and let N_{events}

denote the total number of events uniformly distributed over the full measurement range. Then the relative uncertainty in the estimated differential event density in any given bin obeys

$$\text{Rel. uncertainty} = \frac{\sigma_Q}{Q} \propto \frac{1}{\sqrt{N_{events}}\ \prod_{i=1}^{d} \Delta z_i} \tag{II.4}$$

where Q is the differential quantity (events per unit hypervolume).

Proof. A single histogram bin occupies hypervolume

$$V = \prod_{i=1}^{d} \Delta z_i \tag{II.5}$$

in the measurement space. Under the uniform–density assumption, the expected number of events in that bin scales as

$$N_{bin} \propto N_{events}\, V. \tag{II.6}$$

By Poisson statistics the absolute uncertainty on the bin count is

$$\sigma_{N_{bin}} = \sqrt{N_{bin}}, \tag{II.7}$$

and hence the relative uncertainty on N_{bin} is

$$\frac{\sigma_{N_{bin}}}{N_{bin}} = \frac{1}{\sqrt{N_{bin}}} \propto \frac{1}{\sqrt{N_{events}\, V}} \ . \tag{II.8}$$

Since the differential measurement is $Q = N_{bin}/V$, its relative uncertainty coincides with that of the bin count.

$$\frac{\sigma_Q}{Q} = \frac{(\sigma_{N_{bin}}/V)}{(N_{bin}/V)} \tag{II.9}$$

$$= \frac{\sigma_{N_{bin}}}{N_{bin}} \tag{II.10}$$

$$\propto \frac{1}{\sqrt{N_{events}}\ \prod_{i=1}^{d} \Delta z_i} \ , \tag{II.11}$$

which establishes the claimed scaling. □

This relationship reveals why traditional binned methods become increasingly impractical as dimensionality increases: maintaining fixed statistical precision requires exponentially more data or exponentially coarser binning, both of which severely limit the measurement's resolving power. Beyond a point, the *response matrix*, **R**, becomes not just ill conditioned but genuinely rank deficient, as sufficiently many bins have not just few events in them, but rather no events in them at all. Hence, entire swaths of phase space remain unmeasurable regardless of accumulated statistics.

Binning artifacts compound these statistical challenges through systematic information loss. The process of discretising continuous distributions into finite bins introduces artificial boundaries onto the underlying physics. This discretisation becomes particularly pernicious when dealing with correlation structures that span multiple dimensions. Real particle interactions generate complex kinematic relationships—the angular distribution of decay products correlates with their energies, jet substructure variables depend on the overall jet momentum, and detector response functions couple seemingly independent observables. Binning destroys these correlations by requiring low dimensional projections.

For instance, in jet substructure measurements, the relationship between different substructure variables contains valuable information about the underlying physics that can be obscured by independent binning of each variable. Moreover, many theoretical predictions in particle physics are at the level of statistical moments or other distribution properties rather than full differential spectra. Traditional unfolding methods require first unfolding the full distribution and then calculating these properties, which can lead to reduced precision in the moment predictions.

The computational burden grows even faster than the statistical requirements. Matrix inversion algorithms scale as $\mathcal{O}(N^3)$ with bin number, meaning that the aforementioned four dimensional histogram with 1.6×10^5 bins requires approximately $\mathcal{O}(10^{16})$ floating point operations to invert. More fundamentally, the *null spaces* and *degeneracies* that plague low dimensional unfolding become dramatically worse in higher dimensions, where multiple truth configurations can project to identical detector signatures along numerous measurement axes simultaneously, because high dimensional measurements create complex geometric relationships between true and observed phase spaces.

In addition to these limitations, traditional binned approaches suffer from an additional systematic weakness; the response matrix **R** depends on numerous variables that are typically marginalised over in order to bin the data. While conventional methods construct $\mathbf{R}$ based on a limited set of binned observables, the true detector response depends on a much richer set of event characteristics. These include additional kinematic variables not captured in the chosen binning scheme, event level properties such as particle multiplicity and missing energy, detector conditions like instantaneous luminosity and pileup activity, and correlations with other particles produced in the same collision.

Traditional unfolding methods are effectively forced to assume that $\mathbf{R}$ remains constant when averaged over these marginalised variables, but this assumption is patently incorrect when the detector response varies systematically across different regions of this extended phase space. For example, the energy resolution for jets may depend not only on the jet's transverse momentum and pseudorapidity, variables often chosen for binning, but also on the jet's substructure, the presence of nearby particles, and the overall event topology. By marginalising over these features, binned methods introduce systematic biases that can propagate through the unfolding procedure and distort the final measurements in ways that are difficult to quantify or correct.

II.A.5.ii Unbinned methods.

Unbinned approaches emerge as a natural response to these challenges, operating directly on individual events rather than aggregated histogram counts. These methods exploit the event level structure that binning destroys, preserving the full kinematic information and correlation patterns within each recorded data point. Instead of discretizing phase space into predetermined categories, unbinned techniques allow the data itself to determine the relevant resolution scales and correlation structures.

Rather than explicitly modelling the response function $r(x|z)$, modern techniques like OmniFold [31] employ iterative reweighting strategies that learn implicit mappings between truth and detector-level distributions. These methods sidestep the curse of dimensionality by avoiding explicit probability density estimation, instead focusing on weight optimization that preserves marginal distributions while respecting the detector response.

The computational complexity shifts from matrix algebra to optimization landscapes, that scale more favourably with dimensionality. While traditional unfolding requires inverting matrices that grow exponentially with dimension, unbinned methods typically employ gradient–based optimization that scales polynomially. This trade-off exchanges the well–understood numerical properties of linear algebra for the more complex but ultimately more scalable challenges of machine learning optimization.

Yet this transition introduces new sensitivities to model and hyperparameter choices that traditional methods avoid. The implicit effect of the learning dynamics make it crucial to understand how optimization biases influence the final results. These considerations establish the foundation for exploring how modern machine learning approaches navigate these challenges while preserving the statistical rigour that particle physics demands.

II.B Forward and Inverse Problems in HEP

The measurement process in high-energy physics experiments inherently involves two complementary mathematical challenges: the forward problem of predicting detector responses from particle-level interactions, and the inverse problem of recovering true physics distributions from observed detector measurements. These twin challenges form the conceptual foundation for understanding detector effects and developing unfolding methodologies.

II.B.1 Mathematical Formulation

The relationship between particle–level truth distributions and detector–level observations is governed by the Fredholm integral equation of the first kind [32]

$$p(x) = \int r(x|z)\, p(z)\, \mathrm{d}z + \epsilon(x), \tag{II.12}$$

where $p(z)$ represents the true particle–level distribution, $r(x|z)$ is the detector response kernel encoding resolution effects and acceptance, $p(x)$ is the observed detector-level distribution, and $\epsilon(x)$ accounts for measurement noise [33]. This equation encapsulates the *forward problem* when predicting $p(x)$ given $p(z)$, and the *inverse problem* when estimating $p(z)$ from data $p(x)$.

For discrete histogram representations, this becomes a matrix equation:

$$\boldsymbol{\mu} = \mathbf{R}\boldsymbol{\nu} + \boldsymbol{\epsilon}, \tag{II.13}$$

where $\boldsymbol{\nu}$ and $\boldsymbol{\mu}$ are vectors of true and observed bin counts, respectively, and $\mathbf{R}$ is the smearing matrix containing conditional probabilities $R_{ij} = P(\text{observed bin } i | \text{true bin } j)$ [34].

II.B.2 Challenges in Inverse Problems

The inverse problem in HEP is fundamentally and intrinsically ill–posed. The response kernel is non–injective, i.e. different true distributions can produce identical observed distributions after detector smearing [35, 36]. Furthermore, the distributions are ill–conditioned; small measurement errors

$\boldsymbol{\epsilon}$ amplify into large fluctuations in unfolded solutions due to small singular values in $\mathbf{R}$ [37–39]. These intrinsic challenges with inverse problems are compounded by the fact that modern analyses involve a large number of observables, making brute-force phase space discretization computationally prohibitive [40–42].

These challenges necessitate regularization techniques that impose physical constraints on solutions, such as Tikhonov regularization or iteration cutoffs before convergence, described above.

II.B.3 HEP Specific Considerations

Three aspects particularly complicate unfolding in particle physics compared to other inverse problem domains. First, the response matrix $\mathbf{R}$ is estimated from from detailed Monte Carlo simulations[2] that encode complex, non-Gaussian systematic uncertainties through their modelling assumptions [45–48].

[2] e.g. Pythia [43] for hadronization, Geant4 [44] for detector physics

Second, detector response models contain hundreds to thousands of correlated nuisance parameters—including jet energy scale, b–tagging efficiencies, and pile–up effects-—that must be profiled or marginalized alongside the unfolding procedure [49–52].

Finally, the discrete nature of particle counting combined with highly variable event rates across phase space creates a challenging statistical landscape where Poisson uncertainties dominate in tails and signal regions, while Gaussian approximations may be valid elsewhere [53–56].

A representative unfolding example is differential jet substructure measurements, where detector effects smear the true distribution of observables like jet mass or $N-$subjettiness. The forward problem involves simulating jets through hadronization models and detector response, producing a migration matrix that relates true and reconstructed substructure observables. The inverse problem requires unfolding these observables from reconstructed jets while accounting for correlated uncertainties in jet energy scale, angular resolution, and pile-up contamination [57].

Similar challenges arise in unfolding differential cross sections as functions of transverse momentum, rapidity, or invariant mass, where detector acceptance and resolution vary significantly across the measurement range [58].

II.C Historical development: From matrix inversion to modern approaches

The problem of unfolding has a rich history in high energy physics, with methods evolving alongside computational capabilities and statistical sophistication. Early approaches relied primarily on simple correction factors applied to individual bins of histograms, appropriate only when detector effects were minimal.

As measurements became more precise, regularised matrix inversion techniques emerged as the standard approach. These methods discretise both the particle–level and detector–level distributions into bins, relating them through a response matrix $\mathbf{R}_{ij}$ that describes the probability for an event in particle–level bin j to be observed in detector–level bin i. In component form, Equation (II.13) can be written as

$$\mu_i = \sum_j R_{ij}\nu_j, \tag{II.14}$$

where μ_i is the expected number of counts in detector–level bin i and ν_j is the expected number of events in particle–level bin j. Naively, one might attempt to solve this system by simply inverting the response matrix:

$$\nu_j = \sum_i (R^{-1})_{ji} \mu_i \tag{II.15}$$

However, this direct inversion leads to wildly oscillating solutions with large variances—a manifestation of the ill-posed nature of the unfolding problem. Additionally, R need not, and often is not, a square matrix. To address this issue, a series of techniques were developed to invert Equation (II.13) by imposing additional constraints.

- **Iterative Bayesian unfolding** [59–61]: (also known as Lucy–Richardson deconvolution). Uses Bayes' theorem to iteratively update the estimate of the true distribution, with the number of iterations controlling regularization strength.

- **SVD unfolding** [62]: Applies singular value decomposition to the response matrix and suppresses contributions from small singular values that amplify statistical fluctuations.

- **TUnfold** [63]: Formulates unfolding as a least-squares problem with Tikhonov regularization to penalize large second derivatives, preserving smoothness.

These methods have served the field well for decades, particularly for one–dimensional measurements where binning is manageable. However, they all share the common limitation of requiring discretization of the underlying distributions, which becomes increasingly problematic as measurements probe higher–dimensional spaces and more complex observables.

II.D Traditional unfolding methods in experimental analyses.

Traditional unfolding methods form the bedrock of detector corrections in high-energy physics (HEP), balancing statistical rigour with computational practicality. This section provides an overview of established techniques, their mathematical foundations, implementation nuances, and limitations.

II.D.1 Bin by bin correction.

The simplest unfolding approach applies multiplicative correction factors to observed bin counts:

$$\hat{\nu}_j = \frac{\mu_j - b_j}{C_j}, \quad C_j = \frac{\nu_j^{\mathrm{MC}}}{\mu_j^{\mathrm{MC}}}, \tag{II.16}$$

where μ_j is the observed count in bin j, b_j the estimated background, and C_j the correction factor derived from Monte Carlo (MC) simulations relating particle–level generated (ν_j^{MC}) and detector–level simulated (μ_j^{MC}) events [64].

This method has the advantage of being computationally trivial, with no bin–to–bin correlations. However, it fails to account for a non–diagonal response matrix ($\exists i \neq j : \mathbf{R}_{ij} \neq 0$). This is illustrated most dramatically by the observation that biases persist even with $C_j \to 1$ due to ignored cross–bin migrations [65].

Used primarily in early LHC analyses[3], bin–by–bin correction remains viable only for coarse binnings with negligible migration ($< 5\%$ [34]) between adjacent bins.

II.D.2 Matrix Inversion

When $n_{\text{bins, truth}} = n_{\text{bins, reco}}$, the response matrix $\mathbf{R}$ is square. Formally one can write an unfolded solution as

$$\hat{\boldsymbol{\nu}} = \mathbf{R}^{-1}\boldsymbol{\mu}, \tag{II.17}$$

and even propagate the covariance as

$$V_{\hat{\boldsymbol{\nu}}} = \mathbf{R}^{-1} V_{\boldsymbol{\mu}} (\mathbf{R}^{-1})^T. \tag{II.18}$$

[3]e.g., ATLAS [66, 67] jet cross-sections

However, in practice, direct inversion is highly pathological. This pathology can be quantified by the condition number

$$\kappa(R^{-1}) = \frac{|\lambda_{\max}(R^{-1})|}{|\lambda_{\min}(R^{-1})|} \sim 10^3 - 10^6 \tag{II.19}$$

where $\lambda_{\max}(R^{-1})$ and $\lambda_{\min}(R^{-1})$ are the largest and smallest eigenvalues of R^{-1} respectively. The condition number measures how much a perturbation in the measured counts $\delta\mu$ perturbs the predicted truth counts $\delta\nu$. The large condition number amplifies statistical fluctuations [68, 69]. Further, unphysical solutions such as negative bin count values can arise from noise–dominated eigenvectors.

Methods have been suggested to control this variance, such as Truncated SVD [70], involving discard singular values $\sigma_i < \lambda_{\text{cut}}$ [71], and Wiener-SVD [72], a frequency–domain filtering method to maximize signal–to–noise ratio [73]. Despite this, matrix inversion's instability limits its utility.

II.D.3 Iterative Bayesian unfolding

Bayesian methods regularize through prior distributions $p(z)$, yielding posterior estimates:

$$p(z|x) \propto \mathcal{L}(x|z)p(z) \tag{II.20}$$

Common priors include uniform priors, entropy maximization $p(z) \propto \exp(-\sum z_j \log z_j)$ [74] and Gaussian processes enforcing smoothness [45]. These provide natural uncertainty quantification but suffer from high computational cost, scaling poorly with dimensionality [75],sensitivity to prior misspecification, especially in low-statistics regions [76], and difficulty interpreting credible intervals as frequentist coverage [77].

IBU, also known as Lucy Richardson deconvolution or D'Agostini iterative unfolding [78] is an expectation maximization (EM) algorithm iteratively updates truth estimates

$$\nu_j^{(k+1)} = \nu_j^{(k)} \sum_{i=1}^{N_{\text{Data}}} \frac{R_{ij}\ \mu_i}{\sum_{l=1}^{N_{\text{Truth}}} R_{il}\ \nu_l^{(k)}} \tag{II.21}$$

This method regularises via early stopping, by terminating at $k \sim 4-6$ iterations before noise amplification [79, 80]. The initial guess $\boldsymbol{\nu}^{(0)}$ biases the solution. Some common choices include Generation $\boldsymbol{\nu}_{\mathrm{MC}}$, a uniform distribution, and data driven backwards folding $\mathbf{R}^T\boldsymbol{\mu}$.

While computationally efficient, this approach lacks objective stopping criteria, requiring heuristic cross–validation [81] and underestimates uncertainties due to ignored iteration dependent covariance [82].

IBU is dominant in LHC analyses[4] because it balances simplicity with moderate-dimensional phase spaces ($N_{\mathrm{Truth}} \leq 20$).

II.D.4 Tikhonov Regularization

Tikhonov regularization is a penalized least–squares minimization method

$$\hat{\boldsymbol{\nu}} = \arg\min_{\boldsymbol{\nu}} \left[||\boldsymbol{\mu} - \mathbf{R}\boldsymbol{\nu}||^2 + \lambda ||\mathbf{L}(\boldsymbol{\nu} - \boldsymbol{\nu}_0)||^2 \right] \tag{II.22}$$

[4]e.g. differential jet substructure measurements [83]

where $\mathbf{L}$ is typically the discrete curvature operator[5] and $\boldsymbol{\mu}_0$ a prior estimate [84] that anchors solutions to MC predictions. L-curve optimization balances the residual norm against the solution norm to choose λ [85]. The choice of λ sets the bias variance trade-off. $\lambda \to 0$ represents the high variance, low bias limit and $\lambda \to \infty(\implies \hat{\boldsymbol{\nu}} \to \boldsymbol{\nu}_0)$ represents the low variance, high bias limit. This method is implemented through the TUnfold package, which also provides automated λ tuning via global correlation minimization [63]. However this method struggles with non-differentiable features like threshold effects due to biased curvature penalties, and require ad hoc λ selection via L–curve curvature maximization.

Note. The RooUnfold package [86] provides implemetations of bin–bin–bin corrections, matrix inversion, IBU, SVD, and TUnfold.

[5] e.g. discrete second derivatives

II.D.5 Template Fitting

Template fitting is a method suitable in cases where $N_{\text{Data}} \gg N_{\text{Truth}}$. In this case, one can construct detector–level templates for each truth bin:

$$\mu_i = \sum_{j=1}^{N_{\text{Truth}}} R_{ij}\nu_j + b_i \tag{II.23}$$

with χ^2 minimization:

$$\chi^2 = \sum_{i=1}^{N_{\text{Data}}} \frac{(\mu_i - \sum_j R_{ij}\nu_j - b_i)^2}{\sigma_i^2} \tag{II.24}$$

The solution then is overconstrained, since we leverage $N_{\text{Data}}/N_{\text{Truth}} \sim 2-3$ for stability [87]. Nuisance parameters are systematically modelled via template morphing [88]. Template fitting requires dense detector-level binning, which inflates statistical uncertainties. Template fitting is commonly used in Higgs coupling measurements where broad mass resolutions necessitate wide truth bins.

II.D.6 Regularized Poisson Likelihood

For low-statistics regions, [41] advocates minimizing

$$-\log \mathcal{L}(x \mid z) + \lambda S(z) \tag{II.25}$$

$S(z)$ penalizes non monotonicity in sharply falling spectra. Using cubic B–splines with entropy regularization, this method avoids binning artifacts through continuous representations [41]. However, it requires careful basis function placement to prevent endpoint spikes [89] and demands specialized optimization protocols (e.g., cooling schedules for λ [90]).

II.D.7 Summary

Tab. **??** summarizes the strengths and limitations of the methods discussed above. These limitations motivated the use of machine learning in unfolding, a transition explored in subsequent sections. However, traditional methods remain indispensable for validation and low–dimensional precision measurements where interpretability is crucial.

Method	MC dependence	Uncertainty propagation
Bin–by–bin	Extreme	Underestimated
Matrix inversion	None	Exact but unstable
IBU	Moderate	Partial
Tikhonov	Moderate	Full
Template fit	Low	Full
Regularised Poisson likelihood	Moderate	Full

Table II.1: Comparing the MC dependence and uncertainty propagation of traditional unfolding methods.

II.D.8 Regularization: Need, Approaches, and Limitations

The inherent ill–posedness of unfolding necessitates regularization to stabilize solutions against statistical fluctuations while preserving physical meaning. This section systematically examines the theoretical justification for regularization, surveys dominant methodologies, and critically evaluates their limitations in high energy physics applications.

II.D.8.i The Necessity of Regularization

As discussed earlier, unfolding inverse problems in HEP exhibit pathological characteristics that demand regularization. Regularization counteracts these issues by introducing prior knowledge about $p(z)$, typically favouring smoothness or similarity to Monte Carlo (MC) predictions. However, as Zech and Bohm emphasise in [91], this unavoidably discards information—regularized solutions cannot resolve features finer than the detector resolution or distinguish theories predicting distributions within the regularization bias.

Early termination (typically $k \sim 4 - 6$) acts as implicit regularization by preventing overfitting [92].

II.D.8.ii Limitations and practical challenges

II.D.8.ii.a Subjectivity-objectivity trade-off

All regularization methods inject subjective choices—smoothness scales, prior distributions, stopping criteria and so on——that bias results. This trade–off reveals a deeper epistemological issue: regularization transforms the question from “what does the data show?" to “what does the data show given our assumptions about smoothness?" While Zech [93] and Kuusela [94] argue for publishing unregularized results alongside regularized ones, this approach, though transparent, may be insufficient. The unregularized results often contain artifacts that obscure physical interpretation, and a well chosen regularization scheme can eliminate solutions that are patently unphysical.

A more nuanced approach would involve explicitly testing regularization assumptions against physical models where possible, and developing domain–specific regularization schemes that incorporate known physical constraints rather than generic smoothness priors. This would shift the subjectivity from mathematical convenience to physics–informed choices, making the trade–offs more scientifically meaningful rather than purely computational.

II.D.8.ii.b High dimensional regimes

Traditional methods fail catastrophically in $d \gtrsim 4$ phase spaces for multiple reasons. Binned approaches require n^d histogram bins struggling to effectively sample an increasingly sparse phase space, are shown in Section II.A.5.i.

Global smoothness assumptions become untenable for multi–scale features [62, 95, 96] straining regularization methods that rely on them.

As the number of dimensions increases, the binning also increasingly distorts error propagation. Bayesian credible intervals can exhibit poor frequentist coverage, as shown Fig. 4 of [97], [98, 99], and correlated systematic uncertainties[6] introduce non–convex likelihoods [100, 101].

II.D.8.ii.c Spectrum dependent biases

Sharply falling spectra[7] exacerbate regularization artifacts [41]. Entropic priors overweight high$-z$ regions, distorting tails [103–106], finite sample sizes truncate measurable phase space, creating cutoff–induced spikes [107, 108], and curvature penalties conflict with natural spectral shapes, requiring physics–informed regularization strategies [109–112].

Recent advances aim to mitigate these limitations in various ways. For example, adversarial regularization involves training discriminators to enforce

[6] e.g., jet energy scale

[7] e.g., proton momentum in [102]

physical consistency rather than explicit smoothness̃citeTerjek2019AdversarialRegularization. Differentiable unfolding methods embed detector response in neural networks enabling gradient–based λ optimization [113]. However, no universal solution exists. The choice of regularization must align with analysis–specific priorities, As detector granularity increases, developing dimension–agnostic regularization schemes remains an open challenge requiring collaboration between statisticians and physicists.

II.E Unbinned Methods: Statistical Considerations

The evolution from binned to unbinned unfolding methodologies represents a paradigm shift in high–energy physics, driven by the need to preserve fine–grained kinematic information while managing the statistical and computational complexities of high-dimensional phase spaces. This section systematically analyses the theoretical foundations, practical challenges, and performance trade-offs that this transition entails.

II.E.1 Principles and Implementations

The unbinned approach to unfolding represents a fundamental shift from traditional histogram–based methods. Rather than discretising data into bins, unbinned unfolding preserves the complete kinematic information by operating directly on individual event tuples $\{(z_1, x_1), ..., (z_N, x_N)\}$ where each z_i represents a particle–level event and x_i its corresponding detector–

level measurement. This approach eliminates information loss from binning and naturally handles high–dimensional phase spaces where binning becomes prohibitive.

The central goal of one class of unbinned unfolding methods is to estimate a reweighting function $w(z)$ that transforms the particle–level Monte Carlo distribution, referred to as *generation* (Gen.) to match the underlying truth that was forward folded into the data. Formally, this function satisfies:

$$p(z) = w(z) \cdot q(z), \tag{II.26}$$

where $q(z)$ is the distribution of the generation.

Modern unbinned methods leverage machine learning techniques, particularly those designed for density (ratio) estimation. These approaches fall into two main categories: reweighting methods and direct generative modelling.

II.E.1.i Reweighting Methods

The most established approach in this category is OmniFold, which employs an iterative procedure inspired by the Iterative Bayesian Unfolding

(IBU) algorithm. OmniFold alternates between two steps that estimate likelihood ratios using binary classifiers.

In each iteration k, OmniFold first trains a classifier to distinguish between data and simulated detector–level events, referred to as *simulation* (Sim.), yielding the ratio

$$\nu^{(k)}(x) = \frac{p(x)}{q^{(k)}(x)}, \tag{II.27}$$

where $q^{(k)}(x)$ represents the distribution from simulation weighted by the current iteration's particle–level weights.

This detector–level ratio is then propagated back to particle level through the Monte Carlo pairing. For each generation event z_i with corresponding simulation event x_i, the weight update follows:

$$w^{(k+1)}(z_i) = w^{(k)}(z_i) \cdot \nu^{(k)}(x_i). \tag{II.28}$$

The process, in principle, continues until convergence, at which point the final weights $w(z)$ provide the desired transformation from generation to truth. This connection to likelihood ratio estimation can be explicitly proven—for a binary cross entropy optimized classifier f, the likelihood ratio between the distributions it classifies is

$$LR = \frac{f}{1-f} \tag{II.29}$$

II.E.1.ii Generative Modeling

An alternative approach employs generative models to directly learn the conditional distribution $p(z|x)$. Among these, Conditional Invertible Neural Networks (cINNs) [114] offer a particularly elegant framework.

cINNs learn a diffeomorphic mapping

$$g_\theta : Z \to X \tag{II.30}$$

between particle and detector levels, parameterized by neural network weights θ. The invertibility constraint ensures that for any detector–level observation x, we can directly sample the corresponding particle–level distribution through the inverse mapping. The key advantage lies in the tractable Jacobian computation:

$$p(z|x) = p(x|z)\frac{p(z)}{p(x)} = \left|\det \frac{\partial g_\theta}{\partial z}\right|^{-1} p(g_\theta^{-1}(x)|x), \tag{II.31}$$

enabling direct sampling from the posterior $p(z|x)$ without iterative procedures [115].

Generative models, due to the much greater expressiveness that is necessary for them to model the functional representations needed, are succeptible to training challenges such as mode collapse[8]. Ensuring stable convergence of generative models can get increasingly difficult for high-dimensional problems.

More recently, Schrödinger Bridge Unfolding [116] has emerged as a method that frames unfolding as an optimal transport problem. This approach minimizes the Kullback–Leibler divergence between joint distributions while constraining the marginal to match observed data:

$$\inf_{p(z,x)} D_{\mathrm{KL}}\Big(p(z,x) \parallel p_{\mathrm{MC}}(z,x)\Big) \text{ subject to } p(x) = p_{\mathrm{Data}}(x). \tag{II.32}$$

[8]Normalizing flows however, due to the structural constraints that invertibility imposes, are resistant to mode collapse.

This formulation provides theoretical guarantees on the uniqueness of the solution and offers improved stability compared to purely generative approaches.

II.E.2 Statistical Considerations in Unbinned Regimes

Neural networks implicitly regularize via inductive controls. e.g., convolutional layers enforce translational symmetry in jet images [117]. However, this introduces model–dependent smoothing scales requiring careful validation against closure tests [118].

Reweighting based methods can propagate one part of the overall uncertainty through event weights.

$$\mathrm{Cov}[O] = \sum_{i=1}^{N} w_i^2 O(z_i)^2 - \left(\sum_{i=1}^{N} w_i O(z_i) \right)^2 , \tag{II.33}$$

for observable $O(z)$ [119]. While avoiding binning–induced correlations, unbinned inference requires re–conceptualizing what the unbinned equivalent of the covariance matrix would be in order to appropriately account for correlations in the unfolded data.

II.E.3 Limitations in Complex Phase Spaces

II.E.3.i Model Misspecification

Generative models assume that

$$q(z) > 0 \implies p(z) > 0, \tag{II.34}$$

meaning that wherever generation (particle–level Monte Carlo) assigns positive probability density, $q(z) > 0$, the true distribution also has positive probability density, $p(z) > 0$. This assumption ensures that the generative model does not learn to generate events in regions of phase space where the true physics has zero probability. It is fundamental to the validity of generative unfolding approaches such as conditional Invertible Neural Networks (cINNs) and Variational Autoencoders (VAEs) [120]. Generative models learn to map from detector–level measurements to particle–level distributions by generating samples from the learned posterior. If the generation samples in kinematically forbidden regions or unphysical phase space, the unfolded results will include spurious events that contaminate the measurement. The assumption requires that the generative model be properly constrained to respect the physical boundaries of the true distribution.

Violations of this assumption can occur when generative models, trained on imperfect or limited data, learn to extrapolate beyond the true physical support and generate samples in unphysical regions. This is particularly problematic given the tendency of neural networks to produce overconfident predictions in regions with sparse training data.

Conversely though, enforcing this support containment requirement has practical implications for unfolding performance. Since the generative model can only learn to assign meaningful probability density to regions of phase space adequately represented in the training data, kinematic regimes that are poorly sampled or entirely absent from the Monte Carlo generation are rendered effectively invisible to the unfolding procedure regardless of their importance in the truth distribution. This limitation becomes particularly concerning for new physics searches, where signatures may manifest in previously unexplored regions of phase space. Novel phenomena occurring outside the support of the generative model where cannot be properly unfolded and may remain undetected [121].

The assumption thus places stringent requirements on Monte Carlo coverage and highlights the importance of comprehensive phase space sampling in training data preparation for generative unfolding methods. Hybrid approaches combining discriminative and generative components show promise for anomaly detection [122, 123].

II.F Evaluation metrics for unfolding.

The evaluation of unfolding methods presents unique challenges due to the ill–posed nature of the inverse problem. While the goal of unfolding is conceptually straightforward, to recover the true particle–level distribution from detector–level observations, quantifying the success of this recovery requires careful consideration when the downstream use of the data is unknown. Task–specific evaluation becomes more tractable when clear physics objectives are defined. For example, when unfolding is performed to measure a specific parameter such as α_S, evaluation metrics can be designed to directly assess how well the unfolding procedure enables accurate parameter extraction. This section focuses on metrics and approaches for evaluating unfolding performance, considering both traditional binned techniques and modern unbinned methods, for general–purpose unfolding applications where the downstream use is not known. Metrics for assessing accuracy, precision, and uncertainty quantification are assessed and practical considerations for their application in high energy physics analyses are discussed.

II.F.1 Statistical metrics for evaluating point estimates.

II.F.1.i Residual based metrics.

The most intuitive approach to evaluating an unfolding method is to compare the unfolded distribution to the true distribution when it is known[9]. Simple residual–based metrics quantify the difference between the estimated and true distributions. For binned methods, the bin by bin residual is defined as:

$$\delta_i = \hat{t}_i - t_i \tag{II.35}$$

[9]e.g., in simulation studies

where $\hat{t}_i$ is the unfolded count in bin i and t_i is the true count. Various summary statistics of these residuals can be computed, including

$$\text{MSE} = \frac{1}{n}\sum_{i=1}^{n}(\hat{t}_i - t_i)^2 \tag{II.36}$$

$$\text{RMSE} = \sqrt{\frac{1}{n}\sum_{i=1}^{n}(\hat{t}_i - t_i)^2} \tag{II.37}$$

$$\text{MAE} = \frac{1}{n}\sum_{i=1}^{n}|\hat{t}_i - t_i| \tag{II.38}$$

The MSE might be preferred because it is easier to do calculus with, the RMSE preferred because it is expressed in the units of the original data rather than squared units, but they are manifestly functionally equivalent. The choice between the MSE and MAE depends on the specific requirements of the analysis. MSE more heavily penalizes large errors due to the squaring operation, making it more sensitive to outliers and extreme residuals. MAE treats all errors equally regardless of magnitude and proves more robust to outliers, making it preferable when the unfolding procedure should not be dominated by a few problematic bins or events. The square function though is more amenable to calculus than the absolute value function. In high energy physics applications, RMSE is the most commonly used metric, while MAE may be provided as valuable complementary information.

While these metrics are straightforward, they have limitations in the context of unfolding. In particular, they treat all bins equally, even though certain regions of phase space may be physically more significant than others. Additionally, these metrics do not account for the correlations between bins introduced by the unfolding process.

For unbinned methods, where the output is a set of weights or a continuous probability density, these metrics must be adapted. One approach is to bin the unbinned unfolded distributions and then apply the above metrics, though this introduces binning artifacts that the unbinned method was designed to avoid.

II.F.1.ii Distributional distance metrics.

Given the limitations of simple residual metrics, distributional distance measures provide a more comprehensive assessment of unfolding performance. These metrics compare the entire unfolded distribution to the true distribution.

The *Kullback–Leibler (KL) divergence* [124] measures the information lost when using the unfolded distribution to approximate the true distribution.

$$D_{\mathrm{KL}}(p||q) = \int p(x) \log \frac{p(x)}{q(x)} \, \mathrm{d}x, \tag{II.39}$$

where p is the true distribution and q is the unfolded distribution. While theoretically sound, KL divergence can be numerically unstable when the support of the distributions differs.

The *Vincze–Le Cam (VLC) divergence* [125, 126] is symmetric alternative to KL divergence that is both bounded and highly convex [127].

$$\Delta(p, q) = \frac{1}{2} \int \frac{(p(\lambda) - q(\lambda))^2}{p(\lambda) + q(\lambda)} \, \mathrm{d}\lambda. \tag{II.40}$$

This metric is particularly useful for comparing unfolding methods as it provides a balanced assessment of differences across the entire distribution and has been used in comparative analyses of various unfolding approaches [31, 128].

The *Wasserstein metric* [129], also known as the *Earth mover's distance*," [130] provides a measure of the minimum “work" required to transform one distribution into another.

$$W_p(p,q) = \left(\inf_{\gamma \in \Gamma(p,q)} \int \int |x-y|^p d\gamma(x,y) \right)^{1/p}, \tag{II.41}$$

where $\Gamma(p,q)$ is the set of all joint distributions with marginals p and q. This metric is particularly useful for unfolding evaluations as it accounts for both the magnitude and location of discrepancies between distributions. Table II.2 summarizes the various distributional metrics and their relative strengths for unfolding evaluation.

Table II.2: Distributional distance metrics for unfolding evaluation

	Symmetric	Bounded	Support sensitivity	Compute Cost
D_{KL}	No	No	High	Low
Δ_{VLC}	Yes	Yes	Medium	Low
W_2	Yes	No	Low	High

II.F.2 Uncertainty quantification metrics

Beyond point estimates, properly evaluating unfolding methods requires assessing the accuracy of their uncertainty estimates. This is particularly important in particle physics, where uncertainties propagate to downstream analyses such as parameter fitting.

II.F.2.i Pull distributions

Pull distributions offer a rigorous way to evaluate the calibration of reported uncertainties. For a given unfolded bin or parameter θ, the pull is defined as

$$\mathrm{Pull}\,\theta = \frac{\hat{\theta} - \theta_{\mathrm{true}}}{\sigma_{\hat{\theta}}} \tag{II.42}$$

where $\hat{\theta}$ is the unfolded estimate, θ_{true} is the true value, and $\sigma_{\hat{\theta}}$ is the reported uncertainty. For a well–calibrated method, the pull distribution across many pseudo–experiments should follow a standard normal distribution, $\mathcal{N}(0, 1)$. This follows from the definition of random variables. Since the pull is defined as the ratio of the bias to the estimated uncertainty, for a properly calibrated unfolding method, two conditions must be satisfied simultaneously. First, the method must be unbiased, meaning that across many pseudo experiments, the estimated values should equal the true values on average, resulting in zero mean for the numerator. Second, the reported uncertainties must accurately reflect the actual variability of the estimates, such that the denominator correctly represents the standard deviation of the numerator.

When both conditions are met, the pull becomes a standardized random variable. For sufficiently large sample sizes, many unfolding estimators approach normality due to the Central Limit Theorem, since they often involve weighted sums or averages of many events. When the underlying estimator is approximately normally distributed, if it satisfies the two conditions above that set its mean and standard deviation to 0 and 1 respectively, the population of sample pulls must be distributed as a standard normal.

A pull distribution with non-zero mean indicates systematic bias in the unfolding procedure, Deviations from unit standard deviation indicate either overestimation or underestimation of uncertainties.

In the context of binned unfolding, pull distributions can be computed for each bin, while for unbinned methods, they can be applied to derived quantities or parameters of interest. For Bayesian methods, pulls can be calculated using the mean and standard deviation of the posterior distribution [131].

II.F.2.ii Coverage properties

Related to pulls but more direct is the evaluation of coverage properties of confidence or credible intervals. For a nominal 68% confidence interval, approximately 68% of intervals computed across many pseudo-experiments should contain the true value. Systematic deviations from nominal coverage indicate issues with the uncertainty estimation. Coverage can be assessed through closure tests. These involve generating multiple datasets from a known truth, applying the unfolding procedure, and checking the fraction of times the true value falls within the reported confidence intervals. Coverage plots plot the actual coverage versus the nominal coverage across different confidence levels. The example in Figure II.1 shows expected coverage properties for two different unfolding methods, Tikhonov regularisation and IBU, as a function of the regularisation parameter.

II.F.2.iii Variance and bias decomposition

The total error of an unfolding method can be decomposed into bias and variance components,

$$\mathrm{MSE}(\hat{t}) = \mathrm{Bias}^2(\hat{t}) + \mathrm{Var}(\hat{t}), \tag{II.43}$$

where $\mathrm{Bias}(\hat{t}) = \mathbb{E}[\hat{t}] - t$ and $\mathrm{Var}(\hat{t}) = \mathbb{E}[(\hat{t} - \mathbb{E}[\hat{t}])^2]$.

This decomposition is particularly valuable for understanding the trade–offs inherent in regularized unfolding methods, where stronger regularization typically reduces variance at the expense of increased bias. Different applica-

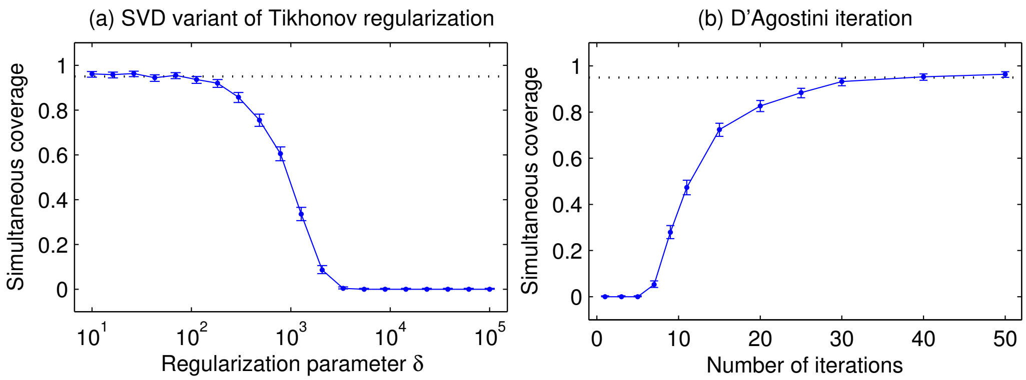

Figure II.1: Coverage of 95% confidence intervals with Tikhonov regularisation (left) and IBU (right). The error bars are given by the 95% Clopper–Pearson intervals and the nominal confidence level is shown by the dotted line. When the regularization is strong (fewer iterations in the case of IBU), both methods undercover substantially. IBU [53]

tions might prioritize minimizing one component over the other, making this decomposition essential for method selection.

II.F.3 Evaluation of correlation structure

Traditional evaluation metrics often focus on marginal distributions, overlooking an important aspect of unfolding: the correlation structure between different bins or events. Properly accounting for these correlations is crucial for downstream analyses.

II.F.3.i Covariance Matrix Assessment

For binned methods, the full covariance matrix of the unfolded distribution provides information about bin–to–bin correlations. A useful measure is the correlation matrix, defined as

$$\mathrm{Corr}_{ij} = \frac{\mathrm{Cov}_{ij}}{\sqrt{\mathrm{Cov}_{ii}\mathrm{Cov}_{jj}}} \tag{II.44}$$

Comparing the correlation structure of the unfolded distribution to that of the true distribution (when known, e.g. in simulation studies) can reveal systematic distortions introduced by the unfolding procedure.

II.F.3.ii Event–to–event correlation metrics

For unbinned methods event–to–event correlations in the unfolded weights can significantly impact downstream inference. These correlations can be quantified by studying the weight correlation as a function of distance. For any pair of events, one can compute the correlation between their weights as a function of their distance in feature space. One can also estimate the reduction in statistical power due to correlated weights

$$N_{\text{eff}} = \frac{\left(\sum_i w_i\right)^2}{\sum_i w_i^2 + 2\sum_{i<j} w_i w_j \mathrm{Corr}(w_i, w_j)} \tag{II.45}$$

In this equation, N_{eff} represents the effective number of independent observations when event weights are correlated, derived from the variance properties of weighted sums. The numerator, $(\sum w_i^2)$ represents the square of the total weighted sample size. The denominator consists of two components, which together account for the increased variance introduced by weight correlations. The first term, $\sum w_i^2$, captures the variance contribution from individual event weights, similar to the standard effective sample size formula for independent weighted observations. The second term, $2\sum_{i<j} w_i w_j \operatorname{Corr}(w_i, w_j)$, accounts for the covariance contributions between all pairs of events, where the factor of 2 arises because each pair appears only once in the sum over $i < j$.

When weights are uncorrelated, $\operatorname{Corr}(w_i, w_j) = 0$, and the formula reduces to the familiar $N_{\text{eff}} = {(\sum w_i)^2}/{\sum w_i^2}$. However, upon unfolding methods, nearby events in phase space often receive similar weight corrections[10], leading to correlations that increase the denominator and reduce the effective sample size. This reduction quantifies the loss of statistical power compared to an ideal scenario with independent weights.

The formula emerges from considering the variance of weighted observables. For a weighted sum, $S = \sum w_i\, x_i$, the variance is

$$\operatorname{Var}(S) = \sum_i \sum_j w_i w_j \operatorname{Cov}(x_i, x_j), \tag{II.46}$$

which is the denominator of the Equation (II.45). The effective sample size is then defined as the ratio of the squared expectation to the variance, providing

[10] as will be discusseed in greater detail in Chapter VII

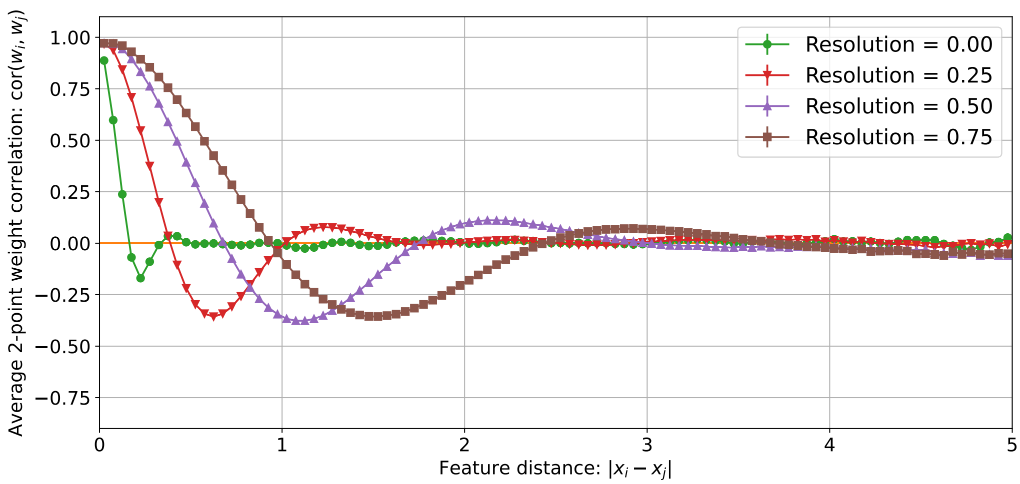

Figure II.2: Average weight correlation between two events as a function of the absolute distance between the events in the observable for Gaussian data unfolded using OmniFold [132].[11]

a measure of statistical efficiency that accounts for both weight magnitudes and their correlations.

Figure II.2 illustrates how event correlations typically decay with distance, with the correlation length scale increasing with detector resolution effects.

[11]Figure created by Owen Long

II.F.4 Method specific evaluation metrics

II.F.4.i Iterative methods

For iterative methods like Iterative Bayesian Unfolding (IBU) or OmniFold, convergence behaviour provides important diagnostic information. To study the convergence behaviour, we plot metric values (e.g., χ^2 or NLL) as a function of iteration number. We then compare unfolded distributions at different iterations to assess stability and analyse how the bias–variance trade off evolves with iteration number.

II.F.4.ii Bayesian Methods

For Bayesian unfolding methods such as Fully Bayesian Unfolding (FBU) [133] or Neural Posterior Unfolding (NPU) [134], additional posterior specific metrics are relevant. We can compare detector level data to detector level predictions generated from the posterior. We assess convergence using standard MCMC based diagnostics like Gelman–Rubin statistics or effective sample size. The width of the posterior allows us to evaluate the posterior uncertainty in relation to the true frequentist variance.

II.F.5 Practical considerations.

In general, when comparing different unfolding methods, a structured evaluation framework ensures fair and comprehensive assessment. Such a framework should consider

- Computational efficiency: Measure training time, inference time, and memory requirements.
- Dimensionality scaling: Assess how performance metrics change as the dimensionality of the problem increases.
- Prior dependence: Evaluate robustness to different initial simulations.
- Regularisation parameter sensitivity: Compare how performance varies with changes in regularization strength.

In real experimental settings where the truth is unknown, evaluation presents additional challenges that require alternative pragmatic approaches. For example, when the true distribution is unavailable, data-splitting techniques can provide useful validation. The two most commonly used techniques are cross-validation, where we split the detector–level data, unfold one portion, then refold it, and compare predictions against the held–out portion; and bootstrapping where we generate multiple resampled datasets to assess the stability of the unfolding procedure.

Closure tests involve applying the full analysis chain (forward model followed by unfolding) to a known input distribution. While not a direct evaluation of performance on real data, closure tests provide confidence in the methodology. The simplest kinds of closure tests involve apply detector simulation to a known particle–level distribution, then unfolding the resulting detector–level distribution and compare with the original input. This procedure can then be modified by using a different particle-level input than the one used to train the unfolding method, testing robustness to prior misspecification.

Evaluating how unfolding methods propagate systematic uncertainties is crucial for real-world applications. We can test the sensitivity of the method to systematic uncertainties by applying variations to the response matrix based on known systematic uncertainties and assessing the impact on unfolded distributions. For methods that support nuisance parameter profiling, evaluating how effectively nuisance parameters are profiled out is a gold standard test for the effectiveness of the method.

Rigorous evaluation of unfolding methods requires a multi–faceted approach that considers accuracy, uncertainty quantification, and computational performance. The metrics and frameworks presented in this section provide a comprehensive foundation for assessing both traditional and machine learning-based unfolding techniques. For binned methods, established metrics like χ^2 and coverage tests remain valuable, while for unbinned approaches, distributional metrics like Wasserstein distance and VLC divergence offer more appropriate evaluation. Regardless of the method, uncertainty calibration through pull distributions and correlation structure assessment are important to validate any measurement. As unfolding methods continue to evolve, particularly with the advent of machine learning approaches, evaluation metrics must adapt accordingly. The framework presented here is designed to be extensible, accommodating new methods and application domains while maintaining rigour and comparability

References

[1] A. Rubbia. *Phenomenology of Particle Physics*. Cambridge, UK: Cambridge University Press, June 2022. ISBN: 978-1-316-51934-9 978-1-009-02342-9.

[2] G. Aad et al. "Observation of a new particle in the search for the Standard Model Higgs boson with the ATLAS detector at the LHC". In: *Phys. Lett. B* 716 (2012), pp. 1–29. DOI: 10.1016/j.physletb.2012.08.020. arXiv: 1207.7214 [hep-ex].

[3] T. C. Collaboration. "Observation of a new boson at a mass of 125 GeV with the CMS experiment at the LHC". In: *Physics Letters B* 716.1

(Sept. 2012). arXiv:1207.7235 [hep-ex], pp. 30–61. ISSN: 03702693. DOI: 10.1016/j.physletb.2012.08.021. URL: http://arxiv.org/abs/1207.7235 (visited on 07/13/2025).

[4] W. Commons. *File:Standard Model of Elementary Particles.svg — Wikimedia Commons, the free media repository.* [Online; accessed 12-July-2025]. 2025. URL: %5Curl%7Bhttps://commons.wikimedia.org/w/index.php?title=File:Standard%5C%5FModel%5C%5Fof%5C%5FElementary%5C%5FParticles.svg&oldid=1013094830%7D.

[5] S. L. Glashow. "Partial Symmetries of Weak Interactions". In: *Nucl. Phys.* 22 (1961), pp. 579–588. DOI: 10.1016/0029-5582(61)90469-2.

[6] S. Weinberg. "Conceptual Foundations of the Unified Theory of Weak and Electromagnetic Interactions". In: *Rev. Mod. Phys.* 52 (1980). Ed. by S. Lundqvist, pp. 515–523. DOI: 10.1103/RevModPhys.52.515.

[7] A. Salam. "Gauge Unification of Fundamental Forces". In: *Rev. Mod. Phys.* 52 (1980). Ed. by A. Ali, C. Isham, T. Kibble, and Riazuddin, pp. 525–538. DOI: 10.1103/RevModPhys.52.525.

[8] P. W. Higgs. “Broken Symmetries and the Masses of Gauge Bosons”. In: *Phys. Rev. Lett.* 13 (16 Oct. 1964), pp. 508–509. DOI: 10.1103/PhysRevLett.13.508. URL: https://link.aps.org/doi/10.1103/PhysRevLett.13.508.

[9] E. D’Hoker and E. Farhi. “Decoupling a fermion in the standard electro-weak theory”. In: *Nuclear Physics, Section B* 248.1 (1984). ISSN: 05503213. DOI: 10.1016/0550-3213(84)90587-x.

[10] Particle Data Group, R. L. Workman, V. D. Burkert, V. Crede, E. Klempt, U. Thoma, L. Tiator, K. Agashe, G. Aielli, B. C. Allanach, et al. “Review of Particle Physics”. In: *Progress of Theoretical and Experimental Physics* 2022.8 (Aug. 2022), p. 083c01. ISSN: 2050-3911. DOI: 10.1093/ptep/ptac097. URL: https://doi.org/10.1093/ptep/ptac097 (visited on 07/13/2025).

[11] A. Chiefa, M. N. Costantini, J. Cruz-Martinez, E. R. Nocera, T. R. Rabemananjara, J. Rojo, T. Sharma, R. Stegeman, and M. Ubiali. “Parton distributions confront LHC Run II data: a quantitative ap-

praisal". en. In: *Journal of High Energy Physics* 2025.7 (July 2025), p. 67. ISSN: 1029-8479. DOI: 10.1007/jhep07(2025)067. URL: https://doi.org/10.1007/JHEP07(2025)067 (visited on 07/13/2025).

[12] "Precision electroweak measurements on the Z resonance". In: *Physics Reports* 427.5 (May 2006), pp. 257–454. ISSN: 0370-1573. DOI: 10.1016/j.physrep.2005.12.006. URL: https://www.sciencedirect.com/science/article/pii/S0370157305005119 (visited on 07/13/2025).

[13] R. Contino, A. Falkowski, F. Goertz, C. Grojean, and F. Riva. "On the validity of the effective field theory approach to SM precision tests". en. In: *Journal of High Energy Physics* 2016.7 (July 2016), p. 144. ISSN: 1029-8479. DOI: 10.1007/jhep07(2016)144. URL: https://doi.org/10.1007/JHEP07(2016)144 (visited on 07/13/2025).

[14] A. Albert, S. Alves, M. André, M. Ardid, S. Ardid, J. .-. J. Aubert, J. Aublin, B. Baret, S. Basa, Y. Becherini, et al. "The ANTARES detector: Two decades of neutrino searches in the Mediterranean Sea". In: *Physics Reports* 1121-1124 (June 2025), pp. 1–46. ISSN: 0370-

1573. DOI: 10.1016/j.physrep.2025.04.001. URL: https://www.sciencedirect.com/science/article/pii/S0370157325001450 (visited on 07/13/2025).

[15] A. Buckley, J. Butterworth, J. Egan, C. Gutschow, S. Jeon, M. Habedank, T. Procter, P. Wang, Y. Yeh, and L. Yue. "Constraints On New Theories Using Rivet : CONTUR version 3 release note". en. In: *arXiv e-prints* (May 2025), arXiv:2505.09272. DOI: 10.48550/arXiv.2505.09272. URL: https://ui.adsabs.harvard.edu/abs/2025arXiv250509272B/abstract (visited on 07/13/2025).

[16] M. E. Peskin and D. V. Schroeder. *An Introduction to quantum field theory*. Reading, USA: Addison-Wesley, 1995. ISBN: 978-0-201-50397-5 978-0-429-50355-9 978-0-429-49417-8. DOI: 10.1201/9780429503559.

[17] S. Navas, C. Amsler, T. Gutsche, W. Vogelsang, C. Hanhart, U. G. Meißner, J. J. Hernández-Rey, A. Pich, C. Lourenço, A. Ceccucci, et al. "Review of particle physics". In: *Physical Review D* 110.3 (Aug. 2024), p. 51. ISSN: 24700029. DOI: 10.1103/physrevd.110.030001. URL:

https://pdg.lbl.gov/2025/reviews/kinematics%5C%5Fand%5C%5Fcross%5C%5Fsections.html.

[18] W. Hollik. "Quantum Field Theory and the Standard ModelQuantum Field Theory and the Standard Model , Matthew D. Schwartz, Cambridge U. Press, 2014. $90.00 (850 pp.). ISBN 978-1-107-03473-0 ". In: *Physics Today* 67.12 (2014), pp. 57–58. ISSN: 0031-9228.

[19] *Quantum Field Theory and the Standard Model* $|CambridgeUniversityPress\&Assessment$. URL: https://www.cambridge.org/us/universitypress/subjects/physics/theoretical-physics-and-mathematical-physics/quantum-field-theory-and-standard-model.

[20] P. E. R. F.R.S. "LXXIX. The scattering of α and β particles by matter and the structure of the atom". In: *The London, Edinburgh, and Dublin Philosophical Magazine and Journal of Science* 21.125 (May 1911), pp. 669–688. ISSN: 1941-5982. DOI: 10.1080/14786440508637080. URL: https://www.tandfonline.com/doi/abs/10.1080/14786440508637080.

[21] W. R. Leo. *Techniques for Nuclear and Particle Physics Experiments: A How-to Approach*. en. Berlin, Heidelberg: Springer, 1994. ISBN: 978-3-540-57280-0 978-3-642-57920-2. DOI: 10.1007/978-3-642-57920-2. URL: https://link.springer.com/10.1007/978-3-642-57920-2 (visited on 07/13/2025).

[22] S. J. Brodsky, F. Fleuret, C. Hadjidakis, and J. P. Lansberg. "Physics opportunities of a fixed-target experiment using LHC beams". In: *Physics Reports* 522.4 (Jan. 2013), pp. 239–255. ISSN: 0370-1573. DOI: 10.1016/j.physrep.2012.10.001.

[23] P. Avery and A. Korytov. "Cross section, Flux, Luminosity, Scattering Rates". In: ().

[24] F. Muheim. "Nuclear and Particle Physics Particle Physics Particle Physics–Measurements and Theory Measurements and Theory Natural Units Relativistic Kinematics Particle Physics Measurements Lifetimes Resonances and Widths Scattering Cross section Collider and Fixed Target Experiments Conservation Laws". In: ().

[25] Belle Collaboration, M. Leitgab, R. Seidl, M. Grosse Perdekamp, A. Vossen, I. Adachi, H. Aihara, D. M. Asner, V. Aulchenko, T. Aushev, et al. "Precision Measurement of Charged Pion and Kaon Differential Cross Sections in ${e}^{+}{e}^{\ensuremath{-}}$ Annihilation at $\sqrt{s}\mathbf{=}10.52\text{ }\text{ }\mathrm{GeV}$". In: *Physical Review Letters* 111.6 (Aug. 2013). Publisher: American Physical Society, p. 062002. DOI: `10.1103/PhysRevLett.111.062002`. URL: `https://link.aps.org/doi/10.1103/PhysRevLett.111.062002` (visited on 07/13/2025).

[26] A. J. Larkoski, I. Moult, and B. Nachman. "Jet substructure at the Large Hadron Collider: A review of recent advances in theory and machine learning". In: *Physics Reports* 841 (Jan. 2020), pp. 1–63. ISSN: 0370-1573. DOI: `10.1016/j.physrep.2019.11.001`.

[27] R. Kogler, B. Nachman, A. Schmidt, L. Asquith, E. Winkels, M. Campanelli, C. Delitzsch, P. Harris, A. Hinzmann, D. Kar, et al. "Jet substructure at the Large Hadron Collider". In: *Reviews of Mod-*

ern Physics 91.4 (Dec. 2019). Publisher: American Physical Society, p. 045003. DOI: `10.1103/RevModPhys.91.045003`. URL: `https://link.aps.org/doi/10.1103/RevModPhys.91.045003` (visited on 07/13/2025).

[28] M. U. Mozer. "Jet reconstruction and substructure measurements in ATLAS and CMS with first Run-2 data". en. In: *Proceedings of Fourth Annual Large Hadron Collider Physics – PoS(LHCP2016)*. Vol. 276. Conference Name: Fourth Annual Large Hadron Collider Physics. SISSA Medialab, Mar. 2017, p. 090. DOI: `10.22323/1.276.0090`. URL: `https://pos.sissa.it/276/090` (visited on 07/13/2025).

[29] "Inverse Problems and Interpretation of Measurements". In: *Applied Mathematical Sciences (Switzerland)* 160 (2005), pp. 1–5. ISSN: 2196968x. DOI: `10.1007/0-387-27132-5{\_}1`.

[30] W. C. Karl. "Regularization in Image Restoration and Reconstruction". In: *Handbook of Image and Video Processing, Second Edition* (Jan. 2005), pp. 183–202. DOI: `10.1016/b978-012119792-6/50075-9`.

[31] A. Andreassen, P. T. Komiske, E. M. Metodiev, B. Nachman, and J. Thaler. "OmniFold: A Method to Simultaneously Unfold All Observables". In: *Physical Review Letters* 124.18 (May 2020). Publisher: American Physical Society, p. 182001. DOI: 10.1103/PhysRevLett.124.182001. URL: https://link.aps.org/doi/10.1103/PhysRevLett.124.182001 (visited on 07/13/2025).

[32] I. Fredholm. "Sur une classe d'équations fonctionnelles". In: *Acta Mathematica* 27.none (Jan. 1903). Publisher: Institut Mittag-Leffler, pp. 365–390. ISSN: 0001-5962, 1871-2509. DOI: 10.1007/bf02421317. URL: https://projecteuclid.org/journals/acta-mathematica/volume-27/issue-none/Sur-une-classe-d%c3%a9quations-fonctionnelles/10.1007/BF02421317.full (visited on 07/13/2025).

[33] S. Weinberg. "Elementary Particle Theory of Composite Particles". In: *Physical Review* 130.2 (Apr. 1963). Publisher: American Physical Society, pp. 776–783. DOI: 10.1103/PhysRev.130.776. URL: https:

//link.aps.org/doi/10.1103/PhysRev.130.776 (visited on 07/13/2025).

[34] CMS Collaboration, S. Chatrchyan, V. Khachatryan, A. M. Sirunyan, A. Tumasyan, W. Adam, T. Bergauer, M. Dragicevic, J. Erö, C. Fabjan, et al. "Measurement of the differential cross section for isolated prompt photon production in pp collisions at 7 TeV". In: *Physical Review D* 84.5 (Sept. 2011). Publisher: American Physical Society, p. 052011. DOI: 10.1103/PhysRevD.84.052011. URL: https://link.aps.org/doi/10.1103/PhysRevD.84.052011 (visited on 07/13/2025).

[35] B. Palumbo, P. Massa, and F. Benvenuto. *Convergence rates for Tikhonov regularization on compact sets: application to neural networks*. arXiv:2505.19936 [math]. May 2025. DOI: 10.48550/arXiv.2505.19936. URL: http://arxiv.org/abs/2505.19936 (visited on 07/13/2025).

[36] A. Neumaier. “Solving Ill-Conditioned and Singular Linear Systems: A Tutorial on Regularization”. In: *SIAM Review* 40.3 (Jan. 1998). Publisher: Society for Industrial and Applied Mathematics, pp. 636–666. ISSN: 0036-1445. DOI: 10.1137/s0036144597321909. URL: https://epubs.siam.org/doi/10.1137/S0036144597321909 (visited on 07/13/2025).

[37] J. Chung and K. Palmer. “A Hybrid Lsmr Algorithm For Large-scale Tikhonov Regularization”. In: (). DOI: 10.1137/140975024. URL: http://www.siam.org/journals/sisc/37-5/97502.html.

[38] J. L. Fernández-Martínez, J. L. G. Pallero, Z. Fernández-Muñiz, and L. M. Pedruelo-González. “The effect of noise and Tikhonov’s regularization in inverse problems. Part I: The linear case”. In: *Journal of Applied Geophysics* 108 (Sept. 2014), pp. 176–185. ISSN: 0926-9851. DOI: 10.1016/j.jappgeo.2014.05.006. URL: https://www.sciencedirect.com/science/article/pii/S0926985114001402 (visited on 07/13/2025).

[39] A. Carpio, O. Dorn, M. Moscoso, F. Natterer, G. C. Papanicolaou, M. L. Rapún, and A. Teta. *Inverse Problems and Imaging*. Ed. by L. L. Bonilla, J. .-. Morel, F. Takens, and B. Teissier. Vol. 1943. Lecture Notes in Mathematics. Berlin, Heidelberg: Springer, 2008. ISBN: 978-3-540-78545-3 978-3-540-78547-7. DOI: 10.1007/978-3-540-78547-7. URL: http://link.springer.com/10.1007/978-3-540-78547-7 (visited on 07/13/2025).

[40] M. Arratia, D. Britzger, O. Long, and B. Nachman. "Optimizing observables with machine learning for better unfolding". en. In: *Journal of Instrumentation* 17.07 (July 2022). Publisher: IOP Publishing, P07009. ISSN: 1748-0221. DOI: 10.1088/1748-0221/17/07/p07009. URL: https://dx.doi.org/10.1088/1748-0221/17/07/P07009 (visited on 07/13/2025).

[41] A. Gaponenko. "A practical way to regularize unfolding of sharply varying spectra with low data statistics". In: *Nuclear Instruments and Methods in Physics Research Section A: Accelerators, Spectrometers,*

Detectors and Associated Equipment 960 (Apr. 2020), p. 163612. ISSN: 0168-9002. DOI: 10.1016/j.nima.2020.163612. URL: https://www.sciencedirect.com/science/article/pii/S0168900220301790 (visited on 07/13/2025).

[42] J. Chan and B. Nachman. “Unbinned profiled unfolding”. In: *Physical Review D* 108.1 (July 2023). Publisher: American Physical Society, p. 016002. DOI: 10.1103/PhysRevD.108.016002. URL: https://link.aps.org/doi/10.1103/PhysRevD.108.016002 (visited on 07/13/2025).

[43] C. Bierlich, S. Chakraborty, N. Desai, L. Gellersen, I. Helenius, P. Ilten, L. Lönnblad, S. Mrenna, S. Prestel, C. T. Preuss, et al. “A comprehensive guide to the physics and usage of PYTHIA 8.3”. In: *SciPost Physics Codebases* (Nov. 2022), p. 8. DOI: 10.21468/SciPostPhysCodeb.8. URL: https://scipost.org/10.21468/SciPostPhysCodeb.8 (visited on 07/13/2025).

[44] J. Allison, K. Amako, J. Apostolakis, P. Arce, M. Asai, T. Aso, E. Bagli, A. Bagulya, S. Banerjee, G. Barrand, et al. "Recent developments in Geant4". In: *Nuclear Instruments and Methods in Physics Research Section A: Accelerators, Spectrometers, Detectors and Associated Equipment* 835 (Nov. 2016), pp. 186–225. ISSN: 0168-9002. DOI: `10.1016/j.nima.2016.06.125`. URL: `https://www.sciencedirect.com/science/article/pii/S0168900216306957` (visited on 07/13/2025).

[45] A. Bozson, G. Cowan, and F. Spanò. "Unfolding with Gaussian Processes". In: (Nov. 2018). _eprint: 1811.01242.

[46] S. Schmitt. "Data Unfolding Methods in High Energy Physics". In: *EPJ Web Conf.* 137 (2017). Ed. by Y. Foka, N. Brambilla, and V. Kovalenko. _eprint: 1611.01927, p. 11008. DOI: `10.1051/epjconf/201713711008`.

[47] V. Blobel. "Unfolding Methods in Particle Physics". In: *Phystat 2011*. Geneva: Cern, 2011, pp. 240–251. DOI: `10.5170/cern-2011-006.240`.

[48] R. G. Huang, A. Cudd, M. Kawaue, T. Kikawa, B. Nachman, V. Mikuni, and C. Wilkinson. "Machine Learning-Assisted Unfolding for Neutrino Cross-section Measurements with the OmniFold Technique". In: (June 2025). DOI: 10.1103/sp1f-n9k2. URL: http://arxiv.org/abs/2504.06857%20http://dx.doi.org/10.1103/sp1f-n9k2.

[49] H. Zhu, K. Desai, M. Kuusela, V. Mikuni, B. Nachman, and L. Wasserman. "Multidimensional Deconvolution with Profiling". In: *NeurIPS. ML4PS*. 150. 2024. DOI: https://doi.org/10.48550/arXiv.2409.10421. arXiv: 0902.0885 [hep-ph].

[50] T. Dorigo and P. de Castro. "Dealing with Nuisance Parameters using Machine Learning in High Energy Physics: a Review". In: (July 2020). URL: https://arxiv.org/abs/2007.09121v2.

[51] K. Cranmer, G. Lewis, L. Moneta, A. Shibata, and W. Verkerke. *HistFactory: A tool for creating statistical models for use with RooFit and RooStats*. New York, 2012. DOI: 10.17181/cern-open-2012-

016. URL: https://cds.cern.ch/record/1456844 (visited on 07/13/2025).

[52] Y. Ke, I. Luise, Q. Buat, and G. Piacquadio. “Recent Developments on the Statistical Treatment of Flavour Tagging Uncertainties in ATLAS”. In: *PoS* Lhcp2022 (2023), p. 322. DOI: 10.22323/1.422.0322.

[53] M. Kuusela and P. B. Stark. “Shape-constrained uncertainty quantification in unfolding steeply falling elementary particle spectra”. In: *The Annals of Applied Statistics* 11.3 (Sept. 2017). Publisher: Institute of Mathematical Statistics, pp. 1671–1710. ISSN: 1932-6157, 1941-7330. DOI: 10.1214/17-aoas1053. URL: https://projecteuclid.org/journals/annals-of-applied-statistics/volume-11/issue-3/Shape-constrained-uncertainty-quantification-in-unfolding-steeply-falling-elementary-particle/10.1214/17-AOAS1053.full (visited on 07/13/2025).

[54] J. Conrad, O. Botner, A. Hallgren, and C. Pérez de los Heros. “Including systematic uncertainties in confidence interval construction for

Poisson statistics". In: *Physical Review D* 67.1 (Jan. 2003). Publisher: American Physical Society, p. 012002. DOI: 10.1103/PhysRevD.67.012002. URL: https://link.aps.org/doi/10.1103/PhysRevD.67.012002 (visited on 07/13/2025).

[55] P. Giovanni and C. Zheng. "Multi-Dimensional Gaussian Fluctuations on the Poisson Space". In: *Electronic Journal of Probability* 15.none (Jan. 2010). Publisher: Institute of Mathematical Statistics and Bernoulli Society, pp. 1487–1527. ISSN: 1083-6489, 1083-6489. DOI: 10.1214/EJP.v15-813. URL: https://projecteuclid.org/journals/electronic-journal-of-probability/volume-15/issue-none/Multi-Dimensional-Gaussian-Fluctuations-on-the-Poisson-Space/10.1214/EJP.v15-813.full (visited on 07/13/2025).

[56] S. G. From and A. W. Swift. "Some New Bounds And Approximations On Tail Probabilities Of The Poisson And Other Discrete Distributions". en. In: *Probability in the Engineering and Informa-*

tional Sciences 34.1 (Jan. 2020), pp. 53–71. ISSN: 0269-9648, 1469-8951. DOI: 10.1017/s0269964818000347. URL: https://www.cambridge.org/core/journals/probability-in-the-engineering-and-informational-sciences/article/abs/some-new-bounds-and-approximations-on-tail-probabilities-of-the-poisson-and-other-discrete-distributions/5D150AD3C15A0F8219340C7437513C3D?utm%5C%5Fsource=chatgpt.com (visited on 07/13/2025).

[57] N. Zardoshti. "Investigating the Role of Coherence Effects on Jet Quenching in Pb-Pb Collisions at \sqrts_NN =2.76 TeV using Jet Substructure". In: *Nucl. Phys. A* 967 (2017). Ed. by U. Heinz, O. Evdokimov, and P. Jacobs. _eprint: 1705.03383, pp. 560–563. DOI: 10.1016/j.nuclphysa.2017.05.055.

[58] G. Cowan. "Statistics for Searches at the LHC". In: *LHC Phenomenology*. Ed. by E. Gardi, N. Glover, and A. Robson. Cham: Springer International Publishing, 2015, pp. 321–355. ISBN: 978-3-319-05361-5 978-3-319-05362-2. DOI: 10.1007/978-3-319-05362-2_9. URL: http:

//link.springer.com/10.1007/978-3-319-05362-2%5C%5F9 (visited on 07/13/2025).

[59] W. H. Richardson. “Bayesian-Based Iterative Method of Image Restoration*”. En. In: *Josa* 62.1 (Jan. 1972). Publisher: Optica Publishing Group, pp. 55–59. DOI: 10.1364/josa.62.000055. URL: https://opg.optica.org/josa/abstract.cfm?uri=josa-62-1-55 (visited on 07/13/2025).

[60] L. B. Lucy. “An iterative technique for the rectification of observed distributions”. en. In: *The Astronomical Journal* 79 (June 1974), p. 745. ISSN: 0004-6256. DOI: 10.1086/111605. URL: https://ui.adsabs.harvard.edu/abs/1974AJ.....79..745L/abstract (visited on 07/13/2025).

[61] S. Schmitt. “Data Unfolding Methods in High Energy Physics”. In: *EPJ Web of Conferences* 137 (Mar. 2017), p. 11008. ISSN: 2100-014x. DOI: 10.1051/epjconf/201713711008. URL: https://www.epj-conferences.org/articles/epjconf/abs/2017/06/epjconf%5C%

5Fconf2017%5C%5F11008/epjconf%5C%5Fconf2017%5C%5F11008.html.

[62] A. Höcker and V. Kartvelishvili. “SVD approach to data unfolding”. In: *Nuclear Instruments and Methods in Physics Research Section A: Accelerators, Spectrometers, Detectors and Associated Equipment* 372.3 (Apr. 1996), pp. 469–481. ISSN: 0168-9002. DOI: 10.1016/0168-9002(95)01478-0. URL: https://www.sciencedirect.com/science/article/pii/0168900295014780 (visited on 07/13/2025).

[63] S. Schmitt. “TUnfold: an algorithm for correcting migration effects in high energy physics”. In: *Jinst* 7 (2012). _eprint: 1205.6201, T10003. DOI: 10.1088/1748-0221/7/10/t10003.

[64] G. Cowan. “Statistics”. In: *Handbook of Particle Detection and Imaging*. Ed. by C. Grupen and I. Buvat. 2021, pp. 103–124. DOI: 10.1007/978-3-319-93785-4_5.

[65] G. Cowan. *Topics in statistical data analysis for high-energy physics.* en. 2010. DOI: 10.5170/cern-2010-002.197. URL: http://cds.cern.ch/record/1281954 (visited on 07/13/2025).

[66] G. Aad, B. Abbott, J. Abdallah, A. A. Abdelalim, A. Abdesselam, O. Abdinov, B. Abi, M. Abolins, H. Abramowicz, H. Abreu, et al. "Measurement of inclusive jet and dijet cross sections in proton-proton collisions at 7 TeV centre-of-mass energy with the ATLAS detector". en. In: *The European Physical Journal C* 71.2 (Feb. 2011), p. 1512. ISSN: 1434-6052. DOI: 10.1140/epjc/s10052-010-1512-2. URL: https://doi.org/10.1140/epjc/s10052-010-1512-2 (visited on 07/13/2025).

[67] *Implications of First LHC Data*. en. URL: https://indico.cern.ch/event/94815/contributions/1282695/ (visited on 07/13/2025).

[68] D. A. Belsley, E. Kuh, and R. E. Welsch. *Regression Diagnostics: Identifying Influential Data and Sources of Collinearity*. en. Google-

Books-ID: GECBEUJVNe0C. John Wiley & Sons, Feb. 2005. ISBN: 978-0-471-72514-5.

[69] M. H. Pesaran. *Time Series and Panel Data Econometrics*. en. Google-Books-ID: 7RokCwAAQBAJ. Oxford University Press, Oct. 2015. ISBN: 978-0-19-105847-9.

[70] H. Deng, Y. Yang, J. Li, C. Chen, W. Jiang, and S. Pu. *Fast Updating Truncated SVD for Representation Learning with Sparse Matrices*. arXiv:2401.09703 [math]. Jan. 2024. DOI: 10.48550/arXiv.2401.09703. URL: http://arxiv.org/abs/2401.09703 (visited on 07/13/2025).

[71] *TruncatedSVD – scikit-learn 1.7.0 documentation*. URL: https://scikit-learn.org/stable/modules/generated/sklearn.decomposition.TruncatedSVD.html.

[72] W. Tang, X. Li, X. Qian, H. Wei, and C. Zhang. "Data Unfolding with Wiener-SVD Method". en. In: *Journal of Instrumentation* 12.10 (Oct. 2017), P10002. ISSN: 1748-0221. DOI: 10.1088/1748-0221/12/

10/p10002. URL: https://dx.doi.org/10.1088/1748-0221/12/10/P10002 (visited on 07/13/2025).

[73] S. Zaroubi. "Wiener reconstruction, SVD and 'optimal' functional bases: Application for redshift galaxy catalogs". In: *30th Rencontres de Moriond: Euroconferences: Clustering in the Universe*. _eprint: astro-ph/9505103. 1995, pp. 135–142.

[74] S. Maeda and T. Iguchi. "A new unfolding code combining maximum entropy and maximum likelihood for neutron spectrum measurement". In: *Journal of Nuclear Science and Technology* 50.4 (Apr. 2013). Publisher: Taylor & Francis _eprint: https://doi.org/10.1080/00223131.2013.773162, pp. 381–386. ISSN: 0022-3131. DOI: 10.1080/00223131.2013.773162. URL: https://doi.org/10.1080/00223131.2013.773162 (visited on 07/13/2025).

[75] G. Cowan. "Bayesian Statistical Methods In Particle Physics". In: *42nd Rencontres de Moriond on QCD and High Energy Hadronic Interactions*. Hanoi, Vietnam: Gioi Publ., 2007, pp. 7–10.

[76] G. Cowan. “Bayesian statistical methods for parton analyses”. In: *14th International Workshop on Deep Inelastic Scattering*. Apr. 2006, pp. 157–160.

[77] F. James, R. Cousins, and G. Cowan. “Statistics”. In: *Phys. Lett. B* 592 (2004), pp. 279–288.

[78] G. D’Agostini. *Improved iterative Bayesian unfolding*. arXiv:1010.0632 [physics]. Oct. 2010. DOI: 10.48550/arXiv.1010.0632. URL: http://arxiv.org/abs/1010.0632 (visited on 07/13/2025).

[79] D. A. Fish, A. M. Brinicombe, E. R. Pike, and J. G. Walker. “Blind deconvolution by means of the Richardson–Lucy algorithm”. En. In: *Josa A* 12.1 (Jan. 1995). Publisher: Optica Publishing Group, pp. 58–65. ISSN: 1520-8532. DOI: 10.1364/josaa.12.000058. URL: https://opg.optica.org/josaa/abstract.cfm?uri=josaa-12-1-58 (visited on 07/13/2025).

[80] L. A. Shepp and Y. Vardi. “Maximum Likelihood Reconstruction for Emission Tomography”. In: *IEEE Transactions on Medical Imaging* 1.2

(Oct. 1982), pp. 113–122. ISSN: 1558-254x. DOI: 10.1109/tmi.1982.4307558. URL: https://ieeexplore.ieee.org/document/4307558 (visited on 07/13/2025).

[81] G. Cowan. “A survey of unfolding methods for particle physics”. In: *Conf. Proc. C* 0203181 (2002). Ed. by M. R. Whalley and L. Lyons, pp. 248–257.

[82] G. Cowan. *Statistical data analysis*. 1998. ISBN: 978-0-19-850156-5.

[83] ATLAS Collaboration, G. Aad, B. Abbott, K. Abeling, N. Abicht, S. Abidi, A. Aboulhorma, H. Abramowicz, H. Abreu, Y. Abulaiti, et al. “Measurement of jet substructure in boosted $t\overline{t}$ events with the ATLAS detector using $140\text{ }\text{ }{\mathrm{fb}}^{\ensuremath{-}1}$ of 13 TeV pp collisions”. In: *Physical Review D* 109.11 (June 2024). Publisher: American Physical Society, p. 112016. DOI: 10.1103/PhysRevD.109.112016. URL: https://link.aps.org/doi/10.1103/PhysRevD.109.112016 (visited on 07/13/2025).

[84] G. Cowan. “Topics in statistical data analysis for HEP”. In: *65th Scottish Universities Summer School in Physics: LHC Physics*. Aug. 2009, pp. 341–369. DOI: 10.1201/b11865-15.

[85] G. Cowan. “Highlights from PHYSTAT 2011”. In: *Phystat 2011*. Geneva: Cern, 2011, pp. 215–224. DOI: 10.5170/cern-2011-006.215.

[86] T. Adye. “Unfolding algorithms and tests using RooUnfold”. In: *Phystat 2011*. _eprint: 1105.1160. Geneva: Cern, 2011, pp. 313–318. DOI: 10.5170/cern-2011-006.313.

[87] D. Britzger. “The Linear Template Fit”. en. In: *The European Physical Journal C* 82.8 (Aug. 2022), p. 731. ISSN: 1434-6052. DOI: 10.1140/epjc/s10052-022-10581-w. URL: https://doi.org/10.1140/epjc/s10052-022-10581-w (visited on 07/14/2025).

[88] M. Baak, S. Gadatsch, R. Harrington, and W. Verkerke. “Interpolation between multi-dimensional histograms using a new non-linear moment morphing method”. In: *Nuclear Instruments and Methods in Physics Research Section A: Accelerators, Spectrometers, Detectors*

and Associated Equipment 771 (Jan. 2015), pp. 39–48. ISSN: 0168-9002. DOI: 10.1016/j.nima.2014.10.033. URL: https://www.sciencedirect.com/science/article/pii/S0168900214011814 (visited on 07/14/2025).

[89] Y. Fan, Y. Li, N. Xue, and D. Ding. "Analysis of Regularized Poisson GLM Spike-Train Modeling". en. In: *Journal of Physics: Conference Series* 2173.1 (Jan. 2022). Publisher: IOP Publishing, p. 012019. ISSN: 1742-6596. DOI: 10.1088/1742-6596/2173/1/012019. URL: https://dx.doi.org/10.1088/1742-6596/2173/1/012019 (visited on 07/14/2025).

[90] J. Jia, F. Xie, and L. Xu. "Sparse Poisson regression with penalized weighted score function". In: *Electronic Journal of Statistics* 13.2 (Jan. 2019). Publisher: Institute of Mathematical Statistics and Bernoulli Society, pp. 2898–2920. ISSN: 1935-7524, 1935-7524. DOI: 10.1214/19-ejs1580. URL: https://projecteuclid.org/journals/electronic-journal-of-statistics/volume-13/issue-2/

Sparse-Poisson-regression-with-penalized-weighted-score-function/10.1214/19-EJS1580.full (visited on 07/14/2025).

[91] G. Bohm and G. Zech. "Introduction to Statistics and Data Analysis for Physicists". In: *Introduction to Statistics and Data Analysis for Physicists* (Aug. 2025). DOI: 10.1142/14343.

[92] H. N. Multhei and B. Schorr. "On an Iterative Method for the Unfolding of Spectra". In: *Nucl. Instrum. Meth. A* 257 (1987), p. 371. DOI: 10.1016/0168-9002(87)90759-5.

[93] G. Zech. "Regularization and error assignment to unfolded distributions". In: *Phystat 2011*. Geneva: Cern, 2011, pp. 252–259. DOI: 10.5170/cern-2011-006.252.

[94] M. J. Kuusela. "Uncertainty quantification in unfolding elementary particle spectra at the Large Hadron Collider". PhD Thesis. Ecole Polytechnique, Lausanne, 2016. DOI: 10.5075/epfl-thesis-7118.

[95] J. L. Fernández-Martínez and Z. Fernández-Muñiz. “The curse of dimensionality in inverse problems”. In: *Journal of Computational and Applied Mathematics* 369 (May 2020), p. 112571. ISSN: 0377-0427. DOI: 10.1016/j.cam.2019.112571. URL: https://www.sciencedirect.com/science/article/pii/S037704271930576X (visited on 07/14/2025).

[96] Y. Xia and N. Zabaras. “Bayesian multiscale deep generative model for the solution of high-dimensional inverse problems”. In: *Journal of Computational Physics* 455 (Apr. 2022), p. 111008. ISSN: 0021-9991. DOI: 10.1016/j.jcp.2022.111008. URL: https://www.sciencedirect.com/science/article/pii/S0021999122000705 (visited on 07/14/2025).

[97] T. Zhang. “A Modification for Bayesian Credible Intervals”. In: *Communications in Statistics - Theory and Methods* 35.9 (Sept. 2006), pp. 1703–1711. ISSN: 03610926. DOI: 10.1080/03610920600683838. URL: https://www.tandfonline.com/doi/abs/10.1080/03610920600683838.

[98] L. E. Eberly and G. Casella. "Estimating Bayesian credible intervals". In: *Journal of Statistical Planning and Inference*. Special issue II: Model Selection, Model Diagnostics, Empirical B ayes and Hierarchical Bayes 112.1 (Mar. 2003), pp. 115–132. ISSN: 0378-3758. DOI: 10.1016/s0378-3758(02)00327-0. URL: https://www.sciencedirect.com/science/article/pii/S0378375802003270 (visited on 07/14/2025).

[99] B. Szabó, A. W. v. d. Vaart, and J. H. v. Zanten. "Frequentist coverage of adaptive nonparametric Bayesian credible sets". In: *The Annals of Statistics* 43.4 (Aug. 2015). arXiv:1310.4489 [math]. ISSN: 0090-5364. DOI: 10.1214/14-aos1270. URL: http://arxiv.org/abs/1310.4489 (visited on 07/14/2025).

[100] N. Berger. "Simplified likelihoods using linearized systematic uncertainties". en. In: *Journal of High Energy Physics* 2023.4 (Apr. 2023), p. 84. ISSN: 1029-8479. DOI: 10.1007/jhep04(2023)084. URL: https://doi.org/10.1007/JHEP04(2023)084 (visited on 07/14/2025).

[101] N. Berger. *Lecture on Statistical analysis methods by ATLAS*. Sept. 2017. URL: https://cds.cern.ch/record/2285058.

[102] G. Arnison, A. Astbury, B. Aubert, C. Bacci, R. Bernabei, A. Bézaguet, R. Böck, T. J. V. Bowcock, M. Calvetti, T. Carroll, et al. "Transverse momentum spectra for charged particles at the CERN proton-antiproton collider". In: *Physics Letters B* 118.1 (Dec. 1982), pp. 167–172. ISSN: 0370-2693. DOI: 10.1016/0370-2693(82)90623-2. URL: https://www.sciencedirect.com/science/article/pii/0370269382906232 (visited on 07/14/2025).

[103] A. Caticha and R. Preuss. "Entropic Priors". In: *AIP Conference Proceedings* 707.1 (Apr. 2004), pp. 371–380. ISSN: 0094-243x. DOI: 10.1063/1.1751380. URL: https://doi.org/10.1063/1.1751380 (visited on 07/14/2025).

[104] C. C. Rodriguez. "Entropic priors for discrete probabilistic networks and for mixtures of Gaussians models". In: *AIP Conference Proceedings* 617.1 (May 2002), pp. 410–432. ISSN: 0094-243x. DOI: 10.1063/1.

1477063. URL: https://doi.org/10.1063/1.1477063 (visited on 07/14/2025).

[105] W. Handley and M. Millea. "Maximum-Entropy Priors with Derived Parameters in a Specified Distribution". In: *Entropy 2019, Vol. 21, Page 272* 21.3 (Mar. 2019), p. 272. ISSN: 1099-4300. DOI: 10.3390/e21030272. URL: https://www.mdpi.com/1099-4300/21/3/272/htm%20https://www.mdpi.com/1099-4300/21/3/272.

[106] B. J. Brewer and M. J. Francis. "Entropic Priors and Bayesian Model Selection". In: *AIP Conference Proceedings* 1193.1 (Dec. 2009), pp. 179–186. ISSN: 0094-243x. DOI: 10.1063/1.3275612. URL: https://doi.org/10.1063/1.3275612 (visited on 07/14/2025).

[107] R. Finotello, V. Lahoche, and D. O. Samary. *Functional Renormalization for Signal Detection: Dimensional Analysis and Dimensional Phase Transition for Nearly Continuous Spectra Effective Field Theory.* arXiv:2507.01064 [physics] version: 1. June 2025. DOI: 10.48550/

arXiv.2507.01064. URL: http://arxiv.org/abs/2507.01064 (visited on 07/14/2025).

[108] E. Marchand and W. E. Strawderman. *On Bayesian credible sets in restricted parameter space problems and lower bounds for frequentist coverage*. arXiv:1208.0028 [math]. Dec. 2012. DOI: 10.48550/arXiv.1208.0028. URL: http://arxiv.org/abs/1208.0028 (visited on 07/14/2025).

[109] Y. Lee and F. C. Park. *On Explicit Curvature Regularization in Deep Generative Models*. arXiv:2309.10237 [cs]. Sept. 2023. DOI: 10.48550/arXiv.2309.10237. URL: http://arxiv.org/abs/2309.10237 (visited on 07/14/2025).

[110] S.-M. Moosavi-Dezfooli, A. Fawzi, J. Uesato, and P. Frossard. *Robustness via curvature regularization, and vice versa*. arXiv:1811.09716 [cs]. Nov. 2018. DOI: 10.48550/arXiv.1811.09716. URL: http://arxiv.org/abs/1811.09716 (visited on 07/14/2025).

[111] G. Zech. "Analysis of distorted measurements – parameter estimation and unfolding". In: (July 2016). _eprint: 1607.06910.

[112] P. Baroň and J. Kvita. "Extending the Fully Bayesian Unfolding with Regularization Using a Combined Sampling Method". In: *Symmetry 2020, Vol. 12, Page 2100* 12.12 (Dec. 2020), p. 2100. ISSN: 2073-8994. DOI: 10.3390/sym12122100. URL: https://www.mdpi.com/2073-8994/12/12/2100/htm%20https://www.mdpi.com/2073-8994/12/12/2100.

[113] E. de la Rosa, D. Robben, D. M. Sima, J. S. Kirschke, and B. Menze. "Differentiable Deconvolution for Improved Stroke Perfusion Analysis". In: *Lecture Notes in Computer Science (including subseries Lecture Notes in Artificial Intelligence and Lecture Notes in Bioinformatics)* 12267 Lncs (2020), pp. 593–602. ISSN: 16113349. DOI: 10.1007/978-3-030-59728-3{_}58/figures/3. URL: https://link.springer.com/chapter/10.1007/978-3-030-59728-3%5C%5F58.

[114] G. Anantha Padmanabha and N. Zabaras. “Solving inverse problems using conditional invertible neural networks”. In: *Journal of Computational Physics* 433 (May 2021), p. 110194. ISSN: 0021-9991. DOI: 10.1016/j.jcp.2021.110194.

[115] M. Bellagente, A. Butter, G. Kasieczka, T. Plehn, A. Rousselot, R. Winterhalder, L. Ardizzone, and U. Köthe. “Invertible Networks or Partons to Detector and Back Again”. In: *SciPost Phys.* 9.5 (Nov. 2020), p. 074. ISSN: 25424653. DOI: 10.21468/scipostphys.9.5.074.

[116] A. Butter, S. Diefenbacher, N. Huetsch, V. Mikuni, B. Nachman, S. P. Schweitzer, and T. Plehn. “Generative unfolding with distribution mapping”. In: *SciPost Phys.* 18.6 (June 2025), p. 200. ISSN: 25424653. DOI: 10.21468/scipostphys.18.6.200.

[117] H. Kheddar, Y. Himeur, A. Amira, and R. Soualah. “Image and Point-cloud Classification for Jet Analysis in High-Energy Physics: A survey”. In: *Frontiers of Physics* 20.3 (Feb. 2025). DOI: 10.15302/frontphys.

2025.035301. URL: http://arxiv.org/abs/2403.11934%20http://dx.doi.org/10.15302/frontphys.2025.035301.

[118] G. Cowan, K. Cranmer, E. Gross, and O. Vitells. "Asymptotic formulae for likelihood-based tests of new physics". In: *Eur.Phys.J.C* 71.2 (Feb. 2011), p. 1554. ISSN: 14346052. DOI: 10.1140/epjc/s10052-011-1554-0.

[119] LHC Higgs Cross Section Working Group, S. Dittmaier, C. Mariotti, G. Passarino, R. Tanaka, S. Alekhin, J. Alwall, E. A. Bagnaschi, A. Banfi, J. Blumlein, et al. "Handbook of LHC Higgs Cross Sections: 2. Differential Distributions". In: (Jan. 2012). DOI: 10.5170/cern-2012-002. URL: http://arxiv.org/abs/1201.3084%20http://dx.doi.org/10.5170/CERN-2012-002.

[120] A. Shmakov, K. Greif, M. J. Fenton, A. Ghosh, P. Baldi, and D. Whiteson. "Full Event Particle-Level Unfolding with Variable-Length Latent Variational Diffusion". In: *SciPost Physics* 18.4 (Jan. 2025). DOI: 10.21468/SciPostPhys.18.4.117. URL: http://arxiv.org/

abs/2404.14332%20http://dx.doi.org/10.21468/SciPostPhys.18.4.117.

[121] C. Amsler, M. Doser, M. Antonelli, D. M. Asner, K. S. Babu, H. Baer, H. R. Band, R. M. Barnett, E. Bergren, J. Beringer, et al. "Monte Carlo techniques". In: *Physics Letters, Section B: Nuclear, Elementary Particle and High-Energy Physics* 667.1-5 (Sept. 2008), pp. 1–6. ISSN: 03702693. DOI: 10.1016/j.physletb.2008.07.018.

[122] F. Di Mattia, P. Galeone, M. De Simoni, and E. Ghelfi. "A Survey on GANs for Anomaly Detection". In: (June 2019). URL: https://arxiv.org/abs/1906.11632v2.

[123] D. Terjék, Terjék, and Dávid. "Adversarial Lipschitz Regularization". In: *arXiv* (Jan. 2019), arXiv:1907.05681. DOI: 10.48550/arxiv.1907.05681. URL: https://ui.adsabs.harvard.edu/abs/2019arXiv190705681T/abstract.

[124] S. Kullback and R. A. Leibler. "On Information and Sufficiency". In: *The Annals of Mathematical Statistics* 22.1 (Mar. 1951). Pub-

lisher: Institute of Mathematical Statistics, pp. 79–86. ISSN: 0003-4851, 2168-8990. DOI: 10.1214/aoms/1177729694. URL: https://projecteuclid.org/journals/annals-of-mathematical-statistics/volume-22/issue-1/On-Information-and-Sufficiency/10.1214/aoms/1177729694.full (visited on 07/14/2025).

[125] I. Vincze. "On the Concept and Measure of Information Contained in an Observation*". In: *Contributions to Probability*. Ed. by J. Gani and V. K. Rohatgi. Academic Press, Jan. 1981, pp. 207–214. ISBN: 978-0-12-274460-0. DOI: 10.1016/b978-0-12-274460-0.50023-0. URL: https://www.sciencedirect.com/science/article/pii/B9780122744600500230 (visited on 07/14/2025).

[126] L. L. Cam. "Asymptotic Methods in Statistical Decision Theory". In: Springer Series in Statistics (1986). DOI: 10.1007/978-1-4612-4946-7. URL: http://link.springer.com/10.1007/978-1-4612-4946-7.

[127] J. Melbourne. “Strongly Convex Divergences”. In: *Entropy* 22.11 (Nov. 2020). arXiv:2009.10838 [cs], p. 1327. ISSN: 1099-4300. DOI: 10.3390/e22111327. URL: http://arxiv.org/abs/2009.10838 (visited on 07/14/2025).

[128] P. Komiske, W. P. McCormack, and B. Nachman. “Preserving new physics while simultaneously unfolding all observables”. In: *Phys. Rev. D* 104.7 (2021). _eprint: 2105.09923, p. 076027. DOI: 10.1103/PhysRevD.104.076027.

[129] *L. N. Vaserstein, “Markov Processes over Denumerable Products of Spaces, Describing Large Systems of Automata”, Probl. Peredachi Inf., 1969, Volume 5, Issue 3,Pages <nobr>64–72</nobr>*. URL: https://m.mathnet.ru/php/archive.phtml?wshow=paper&jrnid=ppi&paperid=1811&option%5C%5Flang=eng.

[130] Y. Rubner, C. Tomasi, and L. Guibas. “A metric for distributions with applications to image databases”. In: *Sixth International Conference on Computer Vision*. Jan. 1998, pp. 59–66. DOI: 10.1109/iccv.1998.

710701. URL: https://ieeexplore.ieee.org/document/710701 (visited on 07/14/2025).

[131] B. T. Knapik, A. W. van der Vaart, and J. H. van Zanten. “Bayesian inverse problems with Gaussian priors”. In: *Annals of Statistics* 39.5 (Feb. 2012), pp. 2626–2657. DOI: 10.1214/11-aos920. URL: http://arxiv.org/abs/1103.2692%20http://dx.doi.org/10.1214/11-AOS920.

[132] K. Desai, O. Long, and B. Nachman. “Unbinned Inference with Correlated Events”. In: *E-print* (Apr. 2025). arXiv: 2504.14072 [physics.data-an].

[133] G. Choudalakis. *Fully Bayesian Unfolding*. arXiv:1201.4612 [physics]. May 2012. DOI: 10.48550/arXiv.1201.4612. URL: http://arxiv.org/abs/1201.4612 (visited on 07/14/2025).

[134] F. T. Acosta, K. Desai, V. Mikuni, B. Nachman, and J. Pan. “Multi-dimensional Deconvolution with Profiling”. In: *NeurIPS. ML4PS*. 177. 2024.